EFEDA-Spain and HAPEX-Sahel

A further analysis of data

M. Soet, J.N.M. Stricker, P. Droogers and J. Esenbrink

Funded by E.C. under contracts: EV5V-CT93-0272
EV5V-CT91-0033

RAPPORT 79 Maart 1998

Afdeling Waterhuishouding
Nieuwe Kanaal 11, 6709 PA Wageningen

ISSN 0926-230X

Contents

List of Tables

List of Figures

0.1 Preface

This report contains the second contribution of the Department of Water Resources to two large field projects financed by the CEC under programme *EPOC-CT 90-0030*

The two projects are EFEDA and HAPEX-Sahel. The first mentioned project was executed in Spain-La Mancha during the period 1991-1994, the second project in Niger during the period 1992-1993.

Both projects were aimed to investigate the role of landsurfaces processes in weather- and climate models. The first part of this report describes additional

fieldwork that had to be done in the EFEDA-area in order to understand the rooting pattern of the vineplants which cover the main part of the arable land. Additional work was undertaken to improve the estimation of the hydraulic properties of the different soils. The results are also presented in this part.

The second part describes results of the HAPEX-Sahel project. Duing the fieldcampaign in Niger a large set of undisturbed soil samples were collected. In the laboratory the hydraulic properties have been determined and analysed. The results are reported here.

We thank Antonio Brasa (University of Castilla-La Mancha, Albacete) for his contribution to the field campaign in March 1994. He made the practical arrangements for our stay in Tomelloso and established a good communication with the landowners. John Bromley and his team (IH, Wallingford) have been very cooperative by realizing the deep drillings at the original EFEDA-I sites. The assistance of Randall Haverkamp (LTHE, Grenoble) during the field work is very much appreciated. The editorial work by Geurtje van Velsen and Peter van Oevelen is greatly appreciated .

Part I

EFEDA-SPAIN

Chapter 1

Introduction

The ECHIVAL (European international project on Climatic and Hydrological Interactions between Vegetation, Atmosphere and Land surface) research program aims at improving the understanding of land surface atmosphere interactions. Part of this program is EFEDA (Echival Field Experiment in a Desertification-threatened Area), which started in 1991 with an intensive field campaign in the region Castilla-La Mancha in Spain (EFEDA-I). The department of Water Resources of the Agricultural University Wageningen was one of the contributors to this experiment. The collected data sets and some preliminary results were reported by [13, Droogers *et al.*, 1993].

The field activities in June 1991 included measurements of soil moisture contents at several sites near Tomelloso, including four vineyards (Appendix 5). The actual evapotranspiration at these sites was measured by teams from different institutes (Table 1.1). The soil profile in this area is characterized by a sandy top layer to about 40 cm depth, overlying a hard calcareous layer of unknown depth. Primarily, it was assumed that root water uptake by the vineplants takes place mainly from the sandy top layer. This assumption was based on the global results of a first fieldtrip in January 1991 and personal communications. Data analysis, however, showed that the amount of soil water depletion over the measured depth (0 — 70 cm) was significantly less than the actual evapotranspiration during identical periods of the field campaign. Therefore, it was concluded that the vine root system probably continues into deeper soil layers.

In 1994 a second, smaller field experiment in the region Castilla-La Mancha has been established in which several institutes participated (EFEDA-II). The contribution of the department of Water Resources to this field experiment had the objective to study both the vine root system and the soil profile in more detail, especially with regard to the characteristics of the calcareous layer. For this study, three vineyards were selected:

- directly north of site TOM2 (due to problems with the owner, measurements at the original site were not possible)

- directly south of site TOM4 (the original vineyard was grubbed up in the period 1991-1994)
- site TOM6.

At each vineyard the root system of one representative plant was excavated. First, the main lateral roots were exposed in order to get information about the symmetry of the root spreading around the plant. Next, the vertical root system was studied in a trench according to the classical method [1, Böhm, 1979]. The exposure of individual roots in the vertical plane appeared to be very difficult due to the hardness of the calcareous layer. Therefore, mainly qualitative information about the vine root system results from this study.

The soil profile is described over the trench depth, which varied from 50 cm (TOM4) to 130 cm (TOM2 and TOM6). At vineyards TOM4 and TOM6, information about deeper soil layers was collected by a team from the Institute of Hydrology (IH) at Wallingford, UK. This team made drillings to about 5.5 m depth at both sites. Additionally, the porosity of undisturbed samples taken from the calcareous layer was determined in the laboratory.

Table 1.1: Contributors to EFEDA-I at Tomelloso sites

site	land use	institute
TOM1	fallow	Water Resources, Wageningen Agricultural University
TOM2	vineyard	Meteorology, Wageningen Agricultural University; Winand Staring Centre, Wageningen
TOM3	vetch	Institute of Hydrology, Wallingford; University of Reading
TOM4	vineyard	Institute of Hydrology, Wallingford
TOM5	vineyard	CNRM, Toulouse
TOM6	vineyard	University of Copenhagen

Another activity during the EFEDA 1991 field campaign was the collection of a large number of soil samples from the top layer. The water retention and hydraulic conductivity curves of these samples were determined by the multi-step outflow method [6, Van Dam *et al.*, 1994]. The results are outlined in appendices 15 to 19 of the report by Droogers *et al.* [13, 1993]. Appendix 19 summarizes the optimized values for the parameters used in the Mualem-Van Genuchten (MVG) model, which describes the water retention and hydraulic conductivity functions [8, Van Genuchten, 1980]. The listed parameter values were determined by inverse modelling of the outflow experiments. In the optimization procedure all MVG-parameters were optimized, except for the saturated moisture content θ_s which was fixed at its measured value. Additional to time-outflow measurements, the moisture contents determined at 15 and 1000 cm pressure were included in the optimization procedure. These points were more or less fixed by setting their weighting factor to 10, whereas the weighting factor for separate time-outflow points equalled 1.

One of the MVG-parameters is the residual moisture content θ_r. When comparing the optimized θ_r values in Appendix 19 for the EFEDA samples

with moisture contents measured in the field, the optimized values were in most cases much higher than measured values. This means, that using the optimized parameter values will cause problems e.g. when simulating field hydrologic processes. The simulated soil profile will then probably remain too wet. The multistep outflow experiments, however, do not provide information for pressures exceeding 1000 cm. In order to obtain this additional information, measurements were made to determine the moisture content at 16000 cm pressure. The resulting $\theta(h = 16000)$ value was included in the optimization runs. After several test runs with different settings a final and definite MVG-parameter set was derived for each sample.

For modelling purposes it is useful to transform this large data set to a meaningful average while preserving the information on spatial variability provided by individual sample results. This can be achieved through the application of geometric scaling theory, based upon the similar media theory originally introduced by Miller and Miller [12, 1956]. Results are presented for simultaneous scaling of soil hydraulic properties using the algorithm described by Clausnitzer *et al.* [4, 1992].

Chapter 2

Material and methods

2.1 Root and soil profile excavation

2.1.1 General information on Tomelloso vineyards

Through personal communication with farmers, general background information was gathered about the vineyard management in the Tomelloso region. Recently, several vineyards in this region were taken out of production and grubbed up, like the 1991 site TOM4. This process will probably continue during the next years, due to European Community rules aiming at reducing the European wine production. In normal circumstances the vineyards may reach an age of up to one hundred years.

Most of the vineplants in the Tomelloso region are of the variety *Aireñ*. The plants in a field form regular grids of 2.5x2.5 m . During the study of the root system, it was observed that the stem of a plant bends horizontally at about 25 cm below the soil surface. According to the farmers this is caused by breaking the stem manually before it is planted. The advantage of creating this horizontal subsurface branch is that more buds become available for sprouting of roots (Fig. 2.1). In general the subsurface branch points in NE-direction away from the stem, thus being shaded by the plant's leaves during the afternoon. Furthermore, the upper soil is regularly cultivated hence no roots will be present in the upper 20 cm.

In addition to the information collected at the selected vineyards, the soil profile and vine root system were studied at a gravel pit about 10 kilometers north of Tomelloso. Part of this gravel pit was located in former vineyards, hence the root system of the vineplants could be easily observed at the vertical walls. Although the soil profile at this location was not representative for the EFEDA sites, the observations provide insight in characteristics like the possible vine rooting depth.

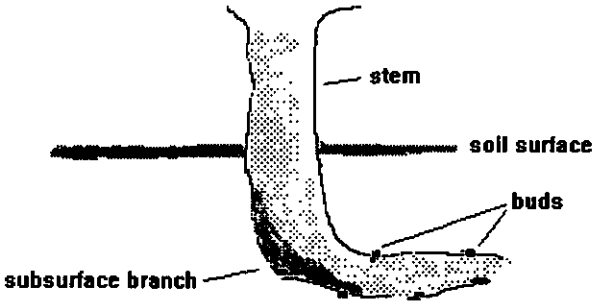

Figure 2.1: Characteristic shape of vineplants in Tomelloso region

2.1.2 Excavation method

The excavation method used in this study was described by Böhm [1, 1979] as the *classical method.* At each vineyard one representative plant was selected at a sufficient distance from the field edge (at least 3 plant rows). The horizontal root pattern was exposed by partly removing the surface layer around the stem. The resulting hole reached to a depth of about 40 cm and had a diameter of about 80 cm. The position of the subsurface branch and the main lateral roots were depicted by drawings and photographs. In order to avoid severe damage to the vineplant, the soil around the stem was replaced before continuing the study of the vertical root system.

After observing the horizontal root distribution, a trench was dug by hand parallel to the subsurface branch, at a distance of about 60 cm from the stem. Its total depth depended upon the soil profile at a specific location: 130 cm at TOM2, 50 cm at TOM4 and 110 cm at TOM6. The length of a trench varied from 1.6 m to 2.4 m, the width was about 60 cm.

The characteristics of the exposed soil layers were described qualitatively. In the EFEDA-I final report, quantitative information about chemical properties and structure for typical soils in the Tomelloso region was given [2, Bolle and Streckenbach, 1993]. To excavate the root system, ideally the soil should be carefully removed from the plant side wall of the trench. For this, a small sharp pointed knife and a brush were used. It appeared to be very difficult however to remove the soil carefully due to the hardness and structure of the calcareous layer. Consequently the root pattern could not be exposed properly and was described mainly qualitative. No attempts were made to determine root lengths, numbers or mass.

At vineyard TOM2 the calcareous layer was somewhat less hard compared to TOM4 and TOM6. Therefore, the vertical root pattern at this site was more easily exposable and root mapping was possible. After brushing the plant side trench wall firmly, it was partly covered by a transparent PVC sheet (length x

width ≈1.3 x 0.85 m) and roots were carefully searched. All visible roots were mapped on the sheet, distinguishing three size classes: > 4 mm, 0.5—4 mm and < 0.5 mm. This root mapping provides a more detailed spatial patterning for the trench at TOM2. To obtain quantitative estimates of total root density in the profile, it would be necessary to calibrate the root map by determining root lengths of small block samples [10, ISRIC, 1992]. Due to the structure of the calcareous layer however block sampling was not possible.

The maximum trench depth was 1.3 meter. Information about deeper soil layers was collected by a team from the Institute of Hydrology, Wallingford UK. They made a deep drilling (to about 5.5 m depth) at the vineyards TOM4 and TOM6, at a distance of about 50 m from the trench in which the root system was studied. During the drilling, disturbed soil samples were collected over 50 cm intervals. In the holes neutron probe access tubes were installed, which were monitored during the summer of 1994. Results will be reported on elsewhere by the Institute of Hydrology.

2.1.3 Porosity measurements

Irregularly shaped fragments from the calcareous layer at vineyards TOM2 and TOM6 were used to estimate the porosity of this layer. Each fragment was split into smaller pieces for porosity and particle density measurements.

First, the dry mass and underwater weight of a crunched sample were measured. From their difference the sample volume can be calculated according to Archimedes' law. Thus, knowing both sample mass and volume, the particle density ρ_s was calculated.

The volume of irregularly shaped pieces was determined accordingly. The samples were weighted dry and after sealing with paraffine weighted underwater. Again the difference between dry and underwater mass yields the sample volume. Once sample volume, mass and particle density were known, the porosity was calculated according to:

$$\phi = 1 - \frac{m}{\rho_s V} \tag{2.1}$$

with ϕ the porosity [$cm^3 cm^{-3}$], m the sample mass [g], ρ_s the particle density [g cm^{-3}] and V the sample volume [cm^3].

2.2 Adjustment of multistep outflow results

2.2.1 Additional moisture content measurements

Moist disturbed samples taken from 19 soil samples used in the multistep outflow method were placed (in duplicate) in a pressure membrane apparatus and subjected to a pressure of 16000 cm for 5 days. Then the gravimetric moisture content w [g g^{-1}] was determined by weighting each sample before and

after ovendrying at 106 °C during 24 hours. The volumetric moisture content θ [cm^3cm^{-3}] was calculated according to:

$$\theta = \frac{\rho_d}{\rho_l} w \tag{2.2}$$

in which ρ_d and ρ_w [g cm^{-3}] are bulk density and density of water respectively. The bulk density was determined as:

$$\rho_d = (1 - \phi)\rho_s \tag{2.3}$$

in which the porosity ϕ was assumed to be equal to the saturated moisture content θ_s and the density of the soil particles ρ_s was taken 2.65 [g cm^{-3}].

2.2.2 Optimization procedure

Estimates of soil hydraulic properties from the multistep outflow method are obtained by inverse modelling of measured time-outflow data. In this inverse method, the flow process is repeatingly simulated with adjusted hydraulic properties until simulated and measured data are sufficiently close. To derive soil hydraulic properties in this way, analytical functions must be used to describe these properties which was in our case the Mualem-Van Genuchten (MVG) model [8, Van Genuchten, 1980]:

$$\Theta = [1 + (a_g |h|)^n]^{-m} \tag{2.4}$$

$$k = k_s \Theta^l \left[1 - \left(1 - \Theta^{1/m}\right)^m\right]^2 \tag{2.5}$$

where $\Theta = (\theta - \theta_r)/(\theta_s - \theta_r)$ and $m = 1 - 1/n$, a_g [cm^{-1}] and n, l [-] are shape parameters, θ_r and θ_s [cm^3cm^{-3}] are residual and saturated water content respectively and k_s [cm h^{-1}] is saturated hydraulic conductivity.

In order to select the best possible optimization procedure for the multistep outflow experiments several test runs were performed. Six samples from the Barrax site, for which the originally optimized θ_r values ranged from 0 to 0.25 [cm^3cm^{-3}] were selected for these runs. Test settings varied for the following properties:

- The weight W assigned to the moisture content value at $h = 1000$ and $h = 16000$ cm pressure. This was done because the θ values obtained after finishing the outflow experiment ($\theta(h = 1000)$) were questioned to represent the correct equilibrium value. Furthermore, the method used to determine the $\theta(h = 16000)$ point is not considered to be very accurate.

- The possible range for optimized θ_r values: no limits, restricted range or fixed value.

The possible range for the MVG-parameters a_g, n, k_s and l was chosen according to the original optimization procedure: $a_g > 0$ [m^{-1}], $1.1 \leq n \leq 5$ [-], $0 < k_s \leq 10$ [$cm\,h^{-1}$] and $-2 \leq l \leq 2.5$ [-]. Initial parameter estimates were identical for all test runs. The setup for the test runs is summarized in Table 2.1. The best possible optimization procedure was selected according to the results of the test runs.

Table 2.1: Setup for test runs

test	$\theta(h = 1000)$	$\theta(h = 16000)$	$\theta_r[cm^3cm^{-3}]$
1	$W = 10$	$W = 4$	free
2	$W = 10$	$W = 10$	free
3	$W = 10$	$W = 0$	≤ 0.05
4	$W = 1$	$W = 10$	free
5	$W = 1$	$W = 0$	≤ 0.05
6	$W = 0$	$W = 1$	$= 0.03$
7	$W = 0$	$W = 0$	$= 0.01$
8	$W = 0$	$W = 1$	$= 0.01$
9	$W = 0$	$W = 10$	$= 0.01$

2.3 Scaling procedure

The application of geometric scaling theory results in a relationship between the water retention and hydraulic conductivity function of sample i with scaled reference curves $h^*(\theta)$ and $k^*(\theta)$:

$$\begin{aligned} h_i &= h^* \alpha_i^{-1} \\ k_i &= k^* \alpha_i^2 \end{aligned} \tag{2.6}$$

The scaling factors α_i and the MVG-parameters for the reference curves were determined using the algorithm described by Clausnitzer *et al.* [4, 1992]. Possible options include scaling of (a) water retention or (b) hydraulic conductivity data only, (c) simultaneous scaling of h and $\ln k$ or (d) simultaneous scaling of $\ln h$ and $\ln k$ as a function of Θ. If options (a) and (b) are applied the calculated set of scaling factors for the retention and conductivity curves may have different statistical properties which is inconsistent with the original similarity theory [4, Clausnitzer et al., 1992]. Therefore, it was chosen to scale both hydraulic properties simultaneously using options (c) and (d) for samples collected at specific sites (if a sufficient number of samples at one site was available), all samples collected at Barrax and all samples collected at Tomelloso. The best scaling option and grouping of samples were selected according to the minimal sum of squared residuals calculated during the scaling procedure.

Chapter 3

Results

3.1 Vine root system and soil profiles

3.1.1 Vineyard TOM2

The selected vineplant was positioned in the vineyard directly north of the 1991 TOM2 site (Fig. 3.1) and had an age of 40 years.

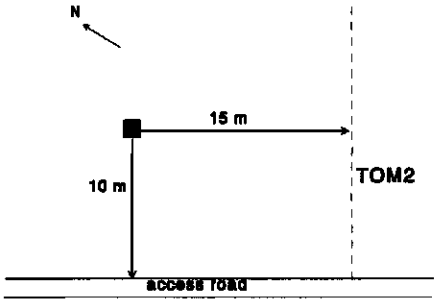

Figure 3.1: Position of vineplant selected near TOM2

The horizontal root system was exposed by removing the top layer around the plant over a circle of 85 cm diameter and a depth of 35 cm. The observed root pattern is shown in Fig. 3.2. The subsurface branch at 25 cm depth pointed in NW-direction and the lateral roots spread equally in all directions from it.

Next a trench of 130 cm depth was dug parallel to the subsurface branch at 65 cm north of the vineplant. Due to the presence of a large lateral root part of the trench reached to a depth of 70 cm only. The soil profile visible in the trench consisted of a sandy top layer to 30 cm depth overlying a calcareous layer reaching to 130 cm depth. The colour of the calcareous layer changed from white to more red with depth, probably due to an increasing iron content (Table

Figure 3.2: Horizontal root system at vineyard TOM2

3.1). Compared to the structure found at vineyard TOM6 the calcareous layer at TOM2 contained more gravel.

At TOM2 no deep drillings were made by the IH-team, hence no exact information is available about deeper soil layers. The structure at the trench bottom, however, indicated that at 130 cm depth a fragmented layer started, consisting of rock fragments and fractures filled with loamy material (see 3.1.2).

Upon hitting the calcareous layer with a chisel, the layer split into thin plates and fragments. Over the entire depth, starting below the subsurface branch, vineroots were observed, but mainly at these splitting surfaces. This leads to a pattern of roots concentrated in horizontal layers. At this site it was feasible to expose the roots properly. The resulting vertical root pattern was mapped at a transparent PVC sheet covering part of the trench wall. A schematized mapping is shown in Fig. 3.3.

3.1.2 Vineyard TOM4

After 1991 the original vineyard was grubbed up and therefore a plant at the vineyard directly south of the 1991 site was selected (Fig. 3.4). This vineyard

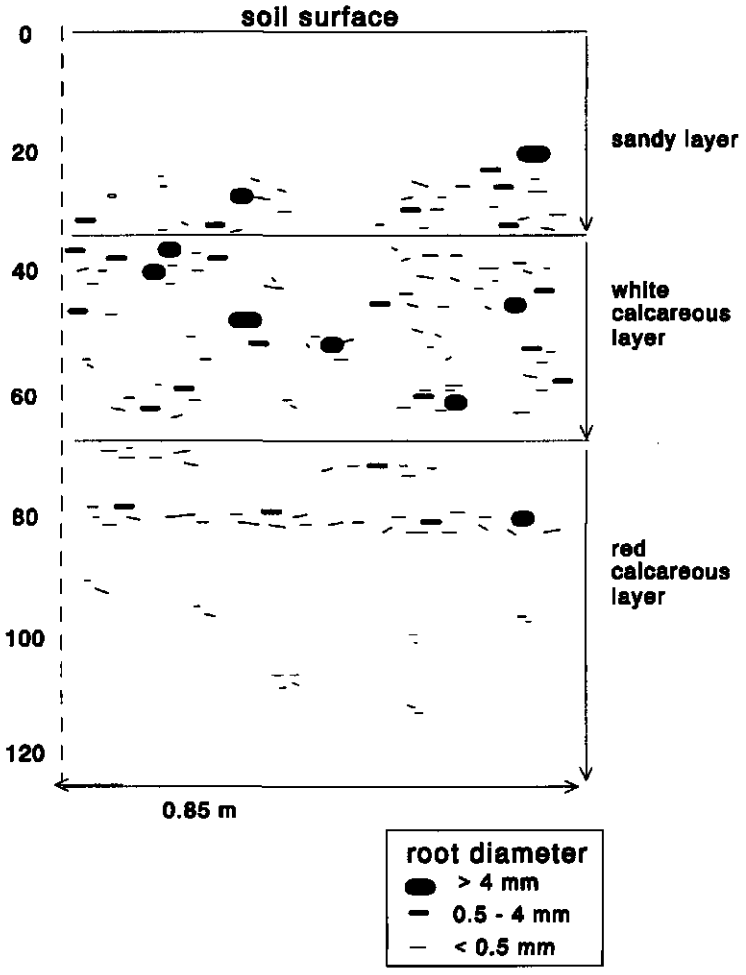

Figure 3.3: Schematized root mapping at vertical trench wall at vineyard TOM2

Table 3.1: Soil profile at vineyard TOM2

depth	description
0-30 cm	sandy layer with gravel
30-65 cm	white calcareous layer with gravel
65-130 cm	gradual transition to darker (red) calcareous layer with a more compact structure
> 130 cm	probably calcareous mudstone

also had an age of 40 years.

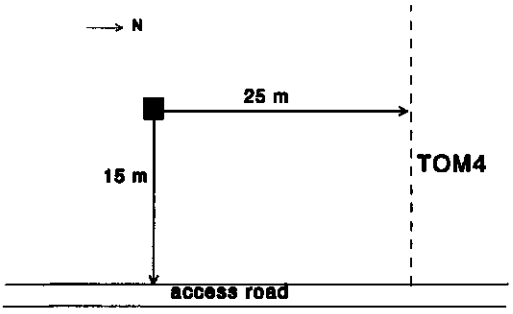

Figure 3.4: Position of vineplant selected near TOM4

The horizontal root system was exposed to a depth of 40 cm. The subsurface branch, at 25 cm depth, pointed in the NE-direction with large lateral roots branching off mainly orthogonally (Fig. 3.5).

For the study of the vertical profile a trench was dug parallel to the subsurface branch. The profile consisted of a sandy top layer till 25 cm depth overlying a calcareous layer that reached from 25 to 50 cm depth. These layers were much more stony than the soil at vineyards TOM2 and TOM6. At 50 cm depth a hard layer formed by rock fragments and fractures filled with loamy material started, which may be classified as *calcareous mudstone* (personal communication Andy Dixon, IH) (Fig. 3.6). In the EFEDA-I final report [2, Bolle and Streckenbach, 1993] a soil description for the Tomelloso region was given. This description mentioned shallow soils (< 10 cm) in the South-Eastern part of the region (uplands) underline by limestones. From there hillsides drop smoothly towards the central plain of the region where the soils are also underlined by hard limestone but deeper. At TOM4, situated about 3 km east of TOM2 and TOM6, these limestones are apparently present at a shallower depth.

At a distance of about 50 m from the trench, a drilling to a depth of 5.4 m was made by the IH-team. The mudstone layer starting at 50 cm depth continued to a depth of 4.9 m. At this depth a shallow clay layer was observed overlying laterite (Table 3.2).

In the sandy top layer hardly any roots were observed, whereas in the calcare-

Figure 3.5: Horizontal root system at vineyard TOM4

ous layer roots were observed regularly. At the bottom of the trench separate rock fragments could be broken out using a chisel. Root growth concentrated in the fractures between these fragments, which are filled with loamy material. Figure 3.7 shows a small rock fragment and the roots growing at the plane of fracture.

3.1.3 Vineyard TOM6

The vineplant selected at this vineyard was situated in the southeastern part of the field (Fig. 3.8). This vineyard had an age of 8 years.

The horizontal root system was exposed to 35 cm depth over a circle of 70 cm diameter. The subsurface branch pointed towards the south instead of in the common NE-direction. Roots spread regularly around the plant and, compared with TOM2 and TOM4, a relatively large number of fine roots was observed (Fig. 3.9). This is probably due to the minor age of this plant.

The trench was dug parallel to the subsurface branch at 55 cm distance from the plant to a depth of 110 cm. The observed soil profile consisted of a sandy top layer to 35 cm depth and a white calcareous layer from 35 to 110 cm depth.

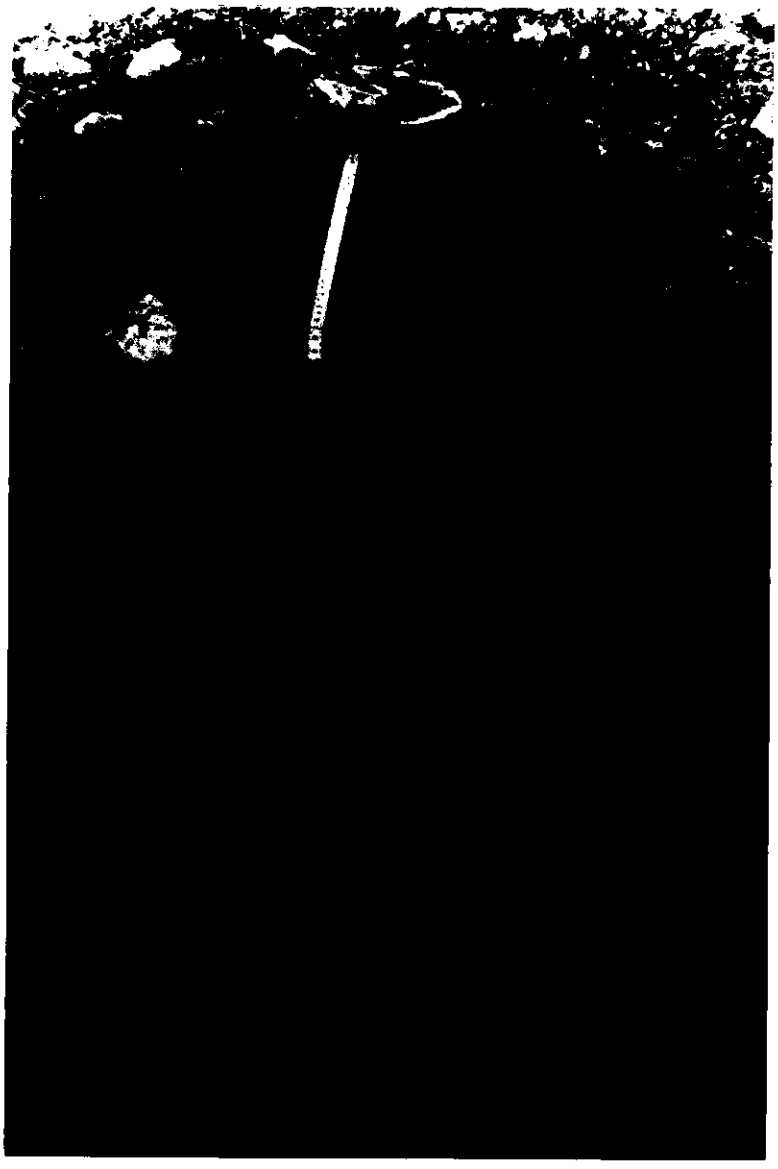

Figure 3.6: Trench at vineyard TOM4 showing mudstone layer starting at 50 cm depth

Table 3.2: Soil profile at vineyard TOM4

depth	description
0-25 cm	sandy layer with gravel
25-50 cm	calcareous layer with gravel
50-490 cm	calcareous mudstone (rock fragments, fractures filled with loamy material)
490-510 cm	soft clay layer
510-540 cm	hard laterite layer

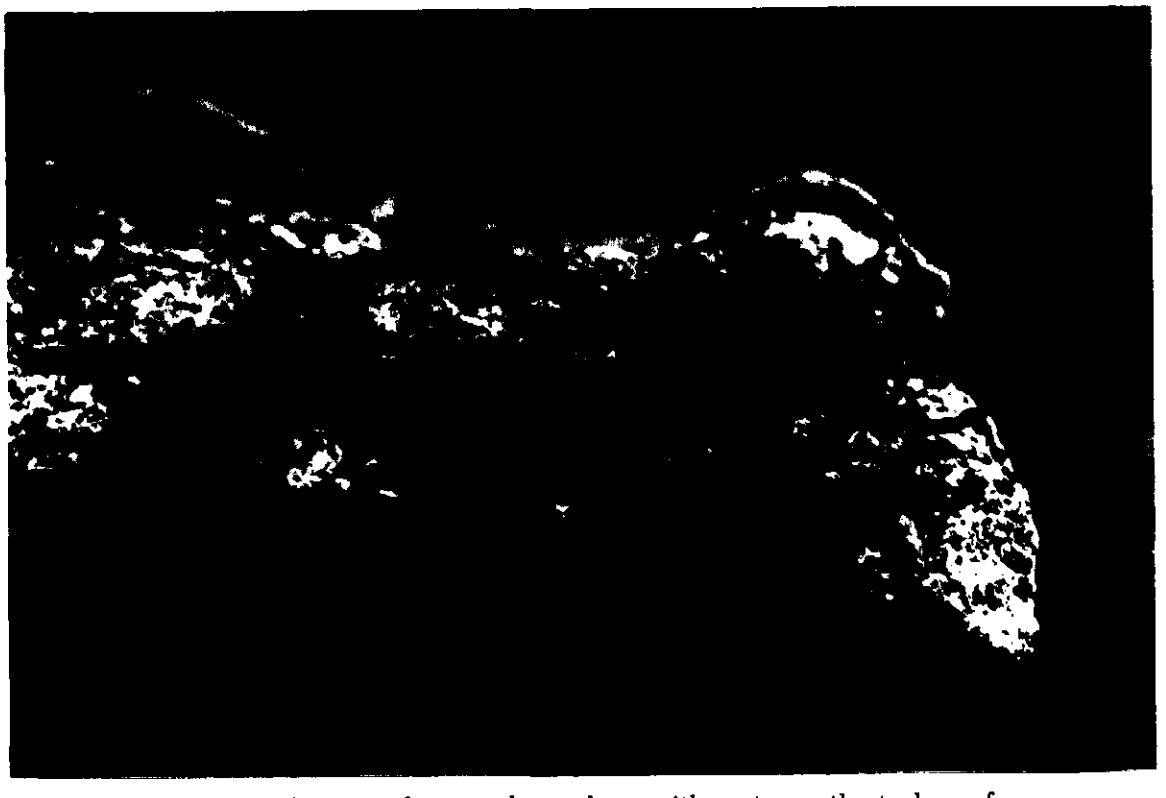

Figure 3.7: Rock fragment from mudstone layer with root growth at plane of fracture

Hand augering at the trench bottom was possible to 145 cm depth, at this depth the soil became apparently much harder. The IH-team made a drilling to 5.5 m depth, which showed that at 150 cm the iron content of the calcareous layer increased (red colour). The calcareous layer continued to 3 m depth. Over this entire depth no gravel was observed, contrary to the observations at TOM2 and TOM4. At 3 m depth a gradual transition from calcareous layer to a mudstone layer was found (Table 3.3).

Roots were observed regularly from 15 to 75 cm depth. Similar to the situation at TOM2, roots concentrated in horizontal layers but relatively more single roots were exposed. Below 75 cm depth, the amount of visible roots was much less but still some were present.

3.1.4 Gravel pit north of Tomelloso

A gravel pit at about 10 km north of Tomelloso, at the road to Pedro Muñoz, was partly situated in former vineyards. The vineroots were still easily observable at the vertical walls of the pit which reached to depths of over 6 meters.

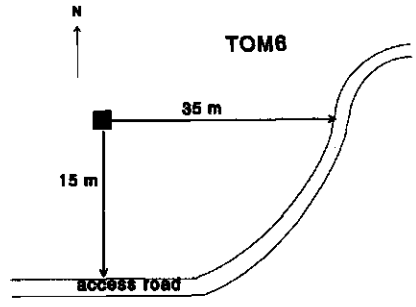

Figure 3.8: Position of vineplant selected at TOM6

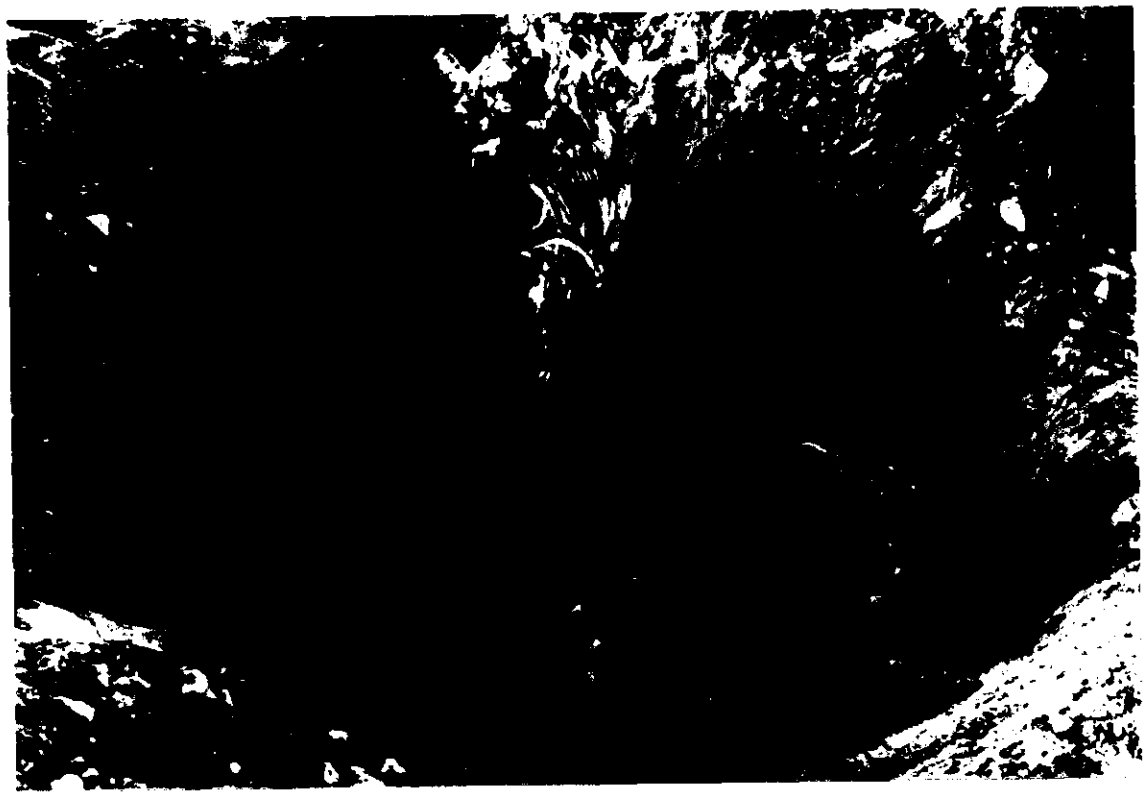

Figure 3.9: Horizontal root system at vineyard TOM6

The soil profile at this location differed from the profiles observed at the EFEDA sites: the calcareous layer starting at about 50 cm depth contained much more gravel than the soils observed at TOM2, TOM4 and TOM6. The thickness of this calcareous layer varied from 30 cm to 100 cm below which again sandy or gravel layers were observed. At some meters depth again compact layers were present but no mudstone layers.

At several locations in the pit, it was observed that the vineroots in a sandy layer spread horizontally directly above a compact calcareous layer. To 4 meters depth roots were regularly present. Figure 3.10 shows a soil profile in the gravel pit with roots growing at about 2 meters depth.

3.1.5 Porosity of calcareous layer

Irregular fragments from the calcareous layer were taken at vineyard TOM2 at 45 cm and 90 cm depth and at TOM6 at 60 cm depth. The particle density and porosity of each fragment were determined in duplicate. Results are given in

Figure 3.10: Soil profile at gravel pit north of Tomelloso with vineroots (red pencil points at vineroots at about 2 m depth)

Table 3.3: Soil profile at vineyard TOM6

depth	description
0-35 cm	sandy layer
35-150 cm	white calcareous layer
150-300 cm	red calcareous layer
300-550 cm	calcareous mudstone

Table 3.4. The average particle density is 2.68 [g cm^{-3}] and the average porosity amounts 0.45 [$cm^3.cm^{-3}$].

Table 3.4: Particle density and porosity of calcareous layer

site	depth [cm]	ρ_s [$g.cm^{-3}$]	ϕ [$cm^3.cm^{-3}$]
TOM2	45	2.687	0.42
TOM2	45	2.688	0.45
TOM2	90	2.677	0.43
TOM2	90	2.687	0.47
TOM6	60	2.678	0.46
TOM6	60	2.678	0.46

3.2 Soil hydraulic properties

3.2.1 Moisture content at 16000 cm pressure

The measured $\theta(h = 16000)$ values are presented in Table 3.5. Additionally the θ_r values derived earlier from the multistep outflow experiments are given. For the sampling locations of the original samples only the field is specified, detailed information about specific plots and sampling depth can be found in appendix 15 of the basic report by Droogers *et al.* [13, 1993].

The average value for Barrax and Tomelloso samples is 0.037 and 0.025 [cm^3cm^{-3}] with a standard deviation of 0.0088 and 0.010 respectively. These values seem quite reasonable since in the field moisture content values of ≈ 0.02 [cm^3cm^{-3}] were measured at site TOM2 [13, Droogers et al., 1993]. The average $\theta(h = 16000)$ values are used further on to select the best optimization procedure for the multistep outflow experiments.

3.2.2 Test runs Barrax

The results of the different test setups given in Table 2.1 may be compared considering:

1. The agreement of measured and simulated time-outflow data represented by the root mean square error RMS.

Table 3.5: Results of moisture content measurements at16000 cm pressure

sample	field	w [g g^{-1}]		θ [cm^{3}cm^{-3}]		$\theta_r$multistep
C10	BAR1	0.020	0.018	0.033	0.030	0.212
A15	BAR1	0.019	0.018	0.031	0.030	0.181
D17	BAR2	0.020	0.022	0.033	0.036	0.046
CT89	BAR3	0.020	0.019	0.029	0.028	0.120
A11	BAR4	0.025	0.028	0.042	0.047	0.257
CT74	BAR5	0.024	0.024	0.040	0.040	0.180
B17	BAR6	0.023	0.024	0.036	0.038	0.216
C11	BAR6	0.024	0.023	0.038	0.036	0.165
B7	BAR8	0.024	-	0.039	-	0.263
D1	BAR9	0.021	0.024	0.033	0.038	0.154
H43	TOM2	0.022	0.019	0.035	0.030	0.163
CT1	TOM2	0.021	-	0.031	-	0.177
H44	TOM2	0.014	0.012	0.020	0.018	0.051
H27	TOM3	0.020	0.020	0.029	0.029	0.195
H45	TOM3	0.019	0.020	0.027	0.029	0.192
H46	TOM3	0.019	-	0.030	-	0.113
H38	TOM3	0.019	0.024	0.030	0.038	0.045
CT13	TOM3	0.014	0.021	0.020	0.030	0.189
H40	TOM3	0.018	0.018	0.028	0.028	0.142

2. The θ value calculated at $h = 16000$ cm.

3. The value of the residual moisture content θ_r.

4. The agreement of optimized retention curves with retention data measured directly in the field [13, Droogers *et al.*, 1993].

In Table 3.6 the test results are represented schematically by means of $++$, $+-$ and $--$ which indicate an overall good fit, poor fit for part of the samples and an overall poor fit of measured data respectively.

Obviously test runs 7 and 8, which differ only in the weighting factor W assigned to the $\theta(h = 16000)$ point, yield overall best results. Simulated and measured time-outflow data resulting from these test runs are shown for two samples in Fig. 3.11. The agreement between optimized retention curves and retention data measured in the field is illustrated in Fig. 3.12.

3.2.3 Revised results for individual samples

To obtain the final set of MVG-parameters for all collected samples, the optimization procedure was run twice for each individual sample using both the settings of test 7 and 8. Checking the results for individual samples in a manner similar to Table 3.6, the settings of test 7 appeared to provide overall best

Table 3.6: Results for test runs Barrax

	time-outflow (1)	$\theta(h = 16000)$ (2)	θ_r (3)	field data (8.4)
test 1	++	−−	++	+−
test 2	−−	−−	−−	−−
test 3	−−	−−	++	−−
test 4	−−	−−	−−	−−
test 5	+−	+−	++	−−
test 6	++	+−	++	+−
test 7	++	+−	++	++
test 8	++	+−	++	++
test 9	++	+−	++	−−

results. Hence for the final parameter set the optimization procedure was performed using the settings of test 7 as given in Table 2.1.

Droogers *et al.* [13, 1993] presented results for 100 cm^3, 250 cm^3 and 600 cm^3 soil samples. Results for the 250 and 600 cm^3 samples, however, showed an overall poor fit of measured and simulated time-outflow data for which no satisfying explanation is available at this moment. Hence only results for 100 cm^3 samples are presented here, yielding a final data set of 66 samples for the Barrax and 20 samples for the Tomelloso sites.

The final MVG-parameter set for individual 100 cm^3 samples is given in Table 3.7. The residual moisture content θ_r equals 0.01 $[cm^3 cm^{-3}]$ for all samples. From Table 3.7 it is obvious that the optimized saturated hydraulic conductivity k_s reaches its upper limit (10 $[cm\,h^{-1}]$) for a relatively large number of samples, in most cases combined with the exponent l reaching its upper limit too. Several attempts were made to get a more realistic distribution of k_s-values like including measured conductivity data (LTHE, Grenoble) or increase the maximum allowed k_s-value during the optimization. This, however, caused conversion problems during the optimization runs or yielded very large k_s- values (up to 100 $[cm\,h^{-1}]$) which seem unrealistic since measured values did not exceed 10 $[cm\,h^{-1}]$. Therefore, the optimized values presented in Table 3.7 are taken as final values but k_s should be considered a fitting parameter rather than a 'true' field value. Finally, Fig. 3.13 illustrates the agreement of optimized water retention curves with suction data measured in the field for an irrigated maize field at Barrax (site BAR5).

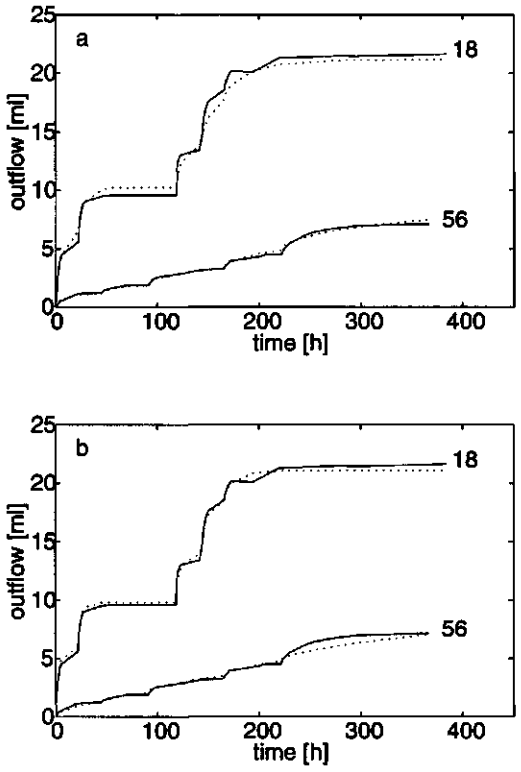

Figure 3.11: Simulated (dotted) and measured (solid lines) time-outflow data for samples 18 and 56 as resulting from test run 7 (a) and test run 8 (b).

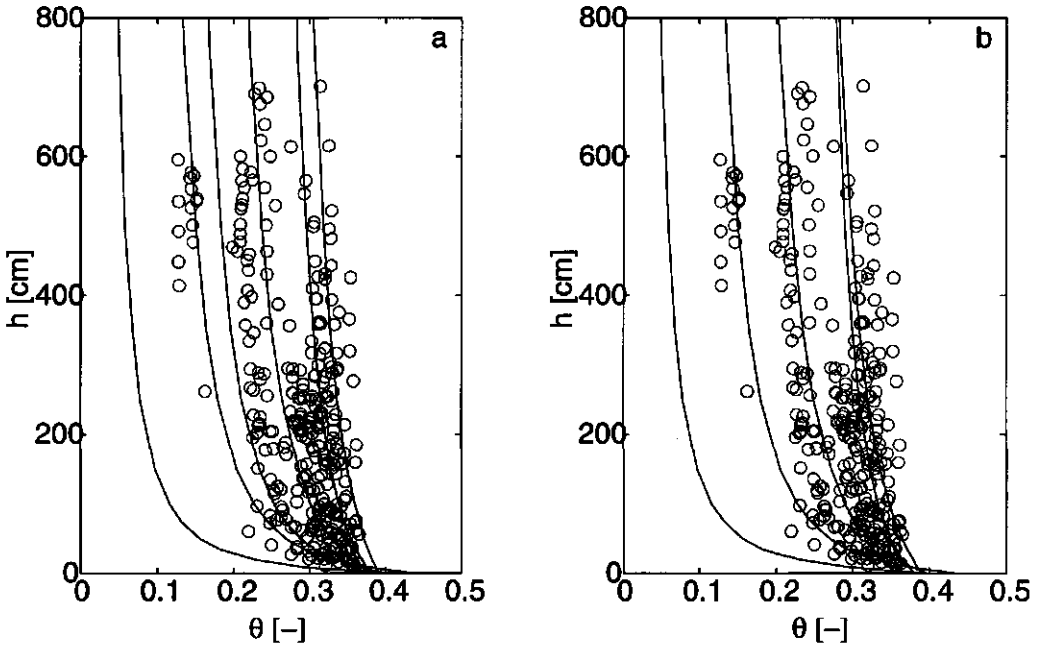

Figure 3.12: Optimized retention curves for 6 test samples (solid lines) resulting from test run 7 (a) and test run 8 (b) and measured field retention data (○).

Table 3.7: Final MVG-parameter set of EFEDA samples 1 to 35

sample	field	plot	depth	a_g	n	θ_s	k_s	l
1	11	1-3	10	0.2470	1.169	0.35	10.00	-1.87
2	11	1-3	10	0.0253	1.150	0.37	3.92	2.50
3	11	1-3	10	0.0556	1.288	0.38	9.75	2.50
4	11	1-3	10	0.0254	1.142	0.38	6.17	2.50
5	11	1-3	10	0.1416	1.428	0.39	10.00	1.12
6	11	1-3	10	0.0412	1.137	0.39	10.00	2.50
7	11	1-3	10	0.0467	1.419	0.42	3.14	2.50
8	11	1-3	10	0.0504	1.451	0.42	10.00	2.50
9	11	1-3	10	0.1688	1.251	0.42	10.00	1.94
10	11	1-3	10	0.0978	1.317	0.44	10.00	2.50
11	11	1-3	20	0.0395	1.100	0.38	9.99	2.50
12	11	1-3	25	0.0345	1.190	0.36	9.98	2.50
13	11	1-3	25	0.0406	1.198	0.37	9.98	2.50
14	11	1-3	25	0.0591	1.199	0.39	9.96	2.50
15	12	6	25	0.0531	1.594	0.40	10.00	-0.14
16	12	6	25	0.0521	1.419	0.40	10.00	0.86
17	12	4-5	25	0.1165	1.422	0.38	6.78	-2.00
18	12	4-5	25	0.1419	1.491	0.40	0.90	-2.00
19	12	4-5	25	0.0963	1.628	0.40	2.60	-2.00
20	14	9-11	10	0.0389	1.100	0.38	10.00	1.81
21	14	9-11	20	0.1406	1.107	0.36	10.00	2.50
22	15	C5	10	0.0391	1.156	0.40	9.83	2.50
23	15	C5	10	0.0409	1.436	0.41	0.16	2.50
24	15	C4	10	0.0128	1.200	0.38	0.03	2.30
25	15	C4	10	0.0247	1.351	0.40	0.04	2.14
26	15	C4	20	0.0321	1.135	0.38	9.97	2.50
27	15	C4	20	0.0377	1.124	0.39	10.00	2.50
28	15	C3	10	0.0370	1.221	0.37	0.18	2.27
29	15	C3	20	0.0479	1.136	0.36	10.00	2.50
30	15	C3	20	0.0472	1.227	0.38	10.00	2.50
31	15	B4	10	0.1349	1.172	0.42	5.13	1.13
32	15	B4	10	0.0628	1.184	0.42	9.91	2.50
33	15	B4	20	0.0369	1.149	0.39	10.00	2.50
34	15	B4	20	0.0549	1.184	0.42	9.99	2.50
35	15	B3	10	0.0919	1.218	0.40	6.84	2.50

Table 3.7: Final MVG-parameter set of EFEDA samples 36 to 70

sample	field	plot	depth	a_g	n	θ_s	k_s	l
36	15	B3	10	0.0953	1.261	0.41	5.10	2.50
37	15	B3	20	0.0484	1.129	0.39	10.00	2.50
38	15	B3	20	0.0886	1.221	0.40	5.78	2.50
39	15	B2	10	0.1054	1.175	0.40	4.08	-0.44
40	15	A3	10	0.0928	1.135	0.40	0.59	-1.54
41	15	A3	10	0.0709	1.132	0.41	1.79	2.50
42	15	A3	20	0.0650	1.139	0.39	4.89	2.50
43	15	A3	20	0.1965	1.100	0.39	10.00	1.41
44	15	A2	10	0.0552	1.228	0.41	0.22	0.60
45	15	A2	10	0.0256	1.254	0.42	0.04	1.83
46	15	A1	20	0.0409	1.267	0.37	0.60	2.50
47	15	12	10	0.0144	1.138	0.37	0.20	-2.00
48	15	12	10	0.0315	1.184	0.38	0.31	-0.06
49	15	12	10	0.0131	1.219	0.40	0.06	2.50
50	15	12	20	0.0247	1.127	0.38	3.32	2.50
51	15	15	10	0.1319	1.222	0.37	9.94	2.50
52	15	15	25	0.0501	1.124	0.38	9.94	2.50
53	15	15	25	0.0622	1.112	0.38	9.99	2.50
54	15	16-20	5	0.0146	1.161	0.41	0.01	2.29
55	15	16-20	20	0.0595	1.115	0.37	10.00	2.50
56	15	16-20	20	0.0149	1.100	0.39	0.04	-1.97
57	16	21-22	10	0.0220	1.231	0.40	7.82	1.68
58	16	21-22	20	0.0215	1.412	0.42	10.00	2.50
59	18	25-27	10	0.0324	1.238	0.39	5.09	2.50
60	18	25-27	10	0.1032	1.438	0.45	10.00	2.50
61	18	25-27	10	0.1032	1.411	0.46	9.98	2.50
62	18	25-27	25	0.0368	1.125	0.38	10.00	2.50
63	18	25-27	25	0.0435	1.138	0.39	5.39	2.50
64	18	25-27	25	0.0357	1.100	0.39	10.00	2.50
65	18	25-27	25	0.1559	1.230	0.41	10.00	2.50
66	19	28	30	0.0133	1.233	0.42	10.00	2.50
67	21	1-2	40	0.0345	1.398	0.43	10.00	2.50
68	22		20	0.0203	1.225	0.41	10.00	2.50
69	22		20	0.0258	1.236	0.45	10.00	2.50
70	22		25	0.0241	1.222	0.40	6.02	2.50

Table 3.7: Final MVG-parameter set of EFEDA samples 71 to 86

sample	field	plot	depth	α_g	n	θ_s	k_s	l
71	22		48	0.0151	1.309	0.46	10.00	2.50
72	22		50	0.0410	1.153	0.43	10.00	1.72
73	22	3	30	0.0241	1.479	0.43	10.00	2.50
74	22	3	50	0.0226	1.394	0.43	10.00	0.81
75	22	3	50	0.0382	1.158	0.43	10.00	2.50
76	22	3	50	0.0201	1.410	0.45	10.00	2.50
77	23	7	10	0.0329	1.323	0.46	10.00	2.50
78	23	7	30	0.0326	1.151	0.40	1.95	-2.00
79	23	9	10	0.0352	1.308	0.39	10.00	2.50
80	23	9	20	0.0118	2.294	0.38	0.003	1.54
81	23	9	25	0.0219	1.483	0.40	10.00	2.50
82	23	9	30	0.0135	1.249	0.33	2.95	1.88
83	23	9	30	0.0349	1.543	0.41	9.97	2.50
84	25		40	0.0180	1.482	0.47	10.00	0.54
85	25	13	30	0.0143	1.298	0.42	3.20	1.84
86	25	13	55	0.0091	1.479	0.46	10.00	2.50

field: 10 = Barrax, 20 = Tomelloso, 1-5 = subsite

3.3 Scaled soil hydraulic properties

The MVG-parameter set for individual samples i (Table 3.7) was used to determine the scaling factors α_i and the reference curves $h^*(\theta)$ and $k^*(\theta)$ through application of the algorithm by Clausnitzer *et al.* [4, 1992]. Scaling was performed for the group of samples collected at BAR1 (1-14), at BAR5 (22-56), all samples from Barrax (1-66) and all samples from Tomelloso (67-86). The minimal sum of squared residuals was obtained when scaling $\ln h$ and $\ln k$ simultaneously over Θ (option (d) in 2.3), hence scaling factors and reference curves resulting from this option are used further on.

The correlation between unscaled original data for sample i and the descaled values estimated from the scaled reference curve and α_i may serve as a measure for the success of the scaling procedure . The correlation between original and descaled soil matric head h and hydraulic conductivity k is plotted for all four groups of samples in Figure 3.14 and 3.15, values of the coefficient of determination R^2 are given in Table 3.8. From Fig. 3.14 and 3.15 and Table 3.8 it is clear that scaling results are satisfactory for soil water retention data when taking the group of samples collected at site BAR1 and site BAR5. Results for all samples collected at the Barrax or Tomelloso sites are relatively poor, especially those for the hydraulic conductivity data. This is probably due to the unrealistic distribution of k_s- values mentioned in 3.2.3. In Fig. 3.14d and 3.15d it can be seen that descaled values for one sample (80) deviate extremely from the 1:1 line which is probably caused by its extremely low k_s-value compared

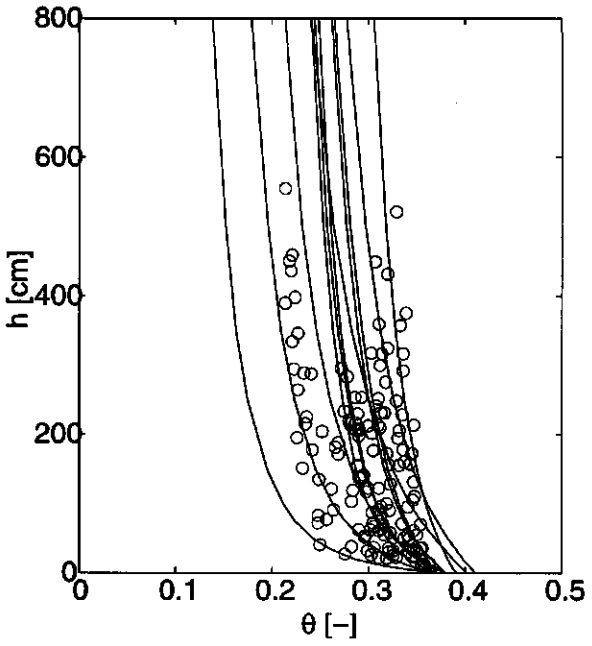

Figure 3.13: Optimized retention curves (solid lines) of samples collected at an irrigated maize field at Barrax (site BAR5) and suction data measured in the field (o).

to other samples from the Tomelloso site.

The MVG-parameters for the scaled reference curves of all four groups of samples are given in Table 9.1. For modelling applications, often the statistical distribution of scaling factors α_i and of the saturated moisture contents θ_s is used. The frequency distributions for α_i and θ_s are shown in Figure 3.16. Application of the Kolmogorov Smirnoff goodness-of-fit test showed that $\ln \alpha$ and θ_s can be taken as normally distributed with mean μ and standard deviation σ at a 0.10 significance level except the $\ln \alpha$ distribution of all combined Barrax samples which was only accepted at the 0.01 level. The parameters characterizing the distributions are given in Table 3.10.

Table 3.8: Coefficient of determination for original versus descaled data

site	sample	$R^2 \log h$	$R^2 \log k$
BAR1	1-14	0.941	0.932
BAR5	22-56	0.958	0.893
Barrax	1-66	0.911	0.792
Tomelloso	67-86	0.899	0.882

Table 3.9: MVG-parameters of scaled reference curves for Barrax and Tomelloso sites

site	depth	a_g	n	θ_r	θ_s	k_s	l
BAR1	0-40 cm	0.0781	1.313	0.01	0.39	8.3	1.9
BAR5	0-40 cm	0.0486	1.219	0.01	0.39	1.5	2.4
Barrax	0-40 cm	0.107	1.312	0.01	0.39	3.2	0.2
Tomelloso	0-40 cm	0.0129	1.427	0.01	0.44	8.8	1.7

Table 3.10: Parameters characterizing the $\ln \alpha$ and θ_s normal distribution

	$\ln \alpha$		θ_s	
site	μ	σ	μ	σ
BAR1	-0.917	1.311	0.390	0.024
BAR5	-0.559	0.947	0.393	0.016
Barrax	-1.530	1.420	0.394	0.021
Tomelloso	-0.331	0.792	0.422	0.026

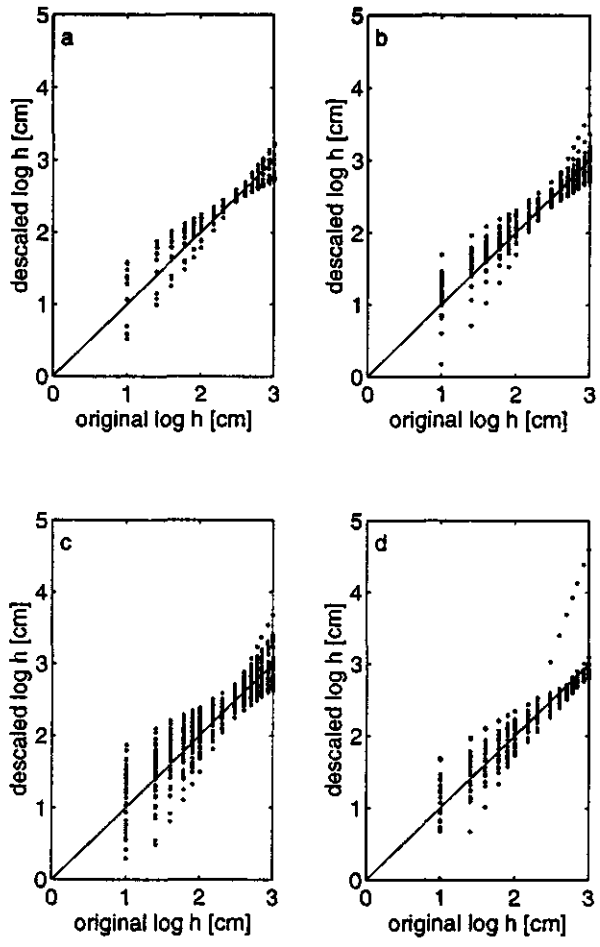

Figure 3.14: Descaled log h values versus original values for the group of samples collected at BAR1 (a), BAR5 (b), Barrax (c) and Tomelloso (d) (solid line = 1:1).

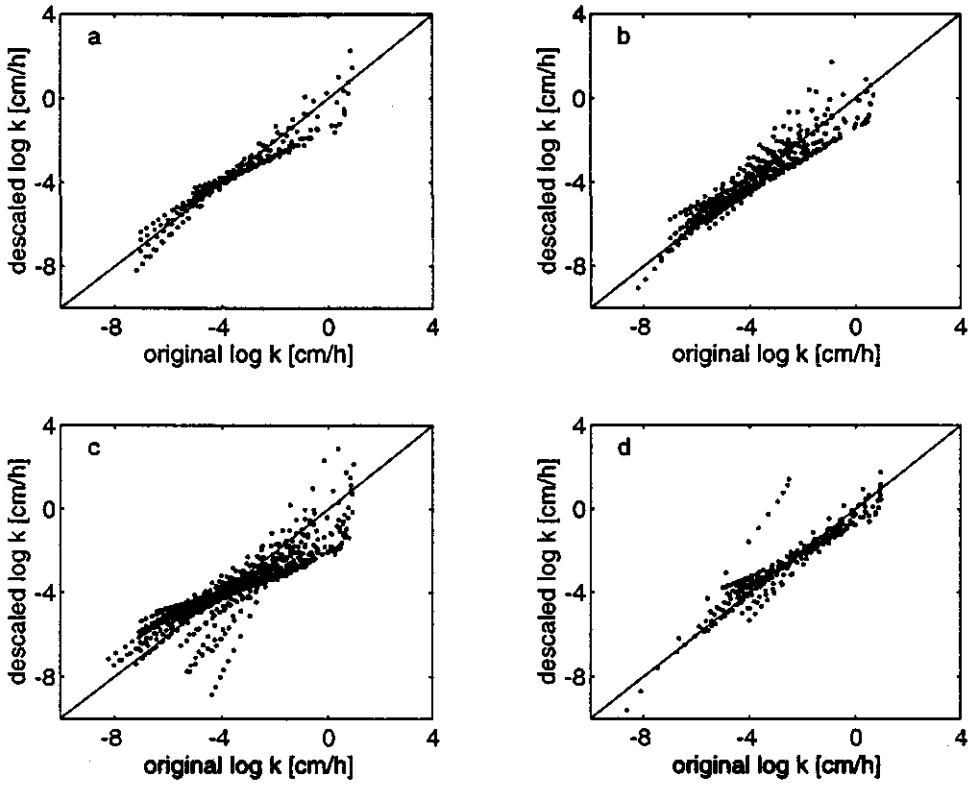

Figure 3.15: Descaled log k values versus original values for the group of samples collected at BAR1 (a), BAR5 (b), Barrax (c) and Tomelloso (d) (solid line = 1:1).

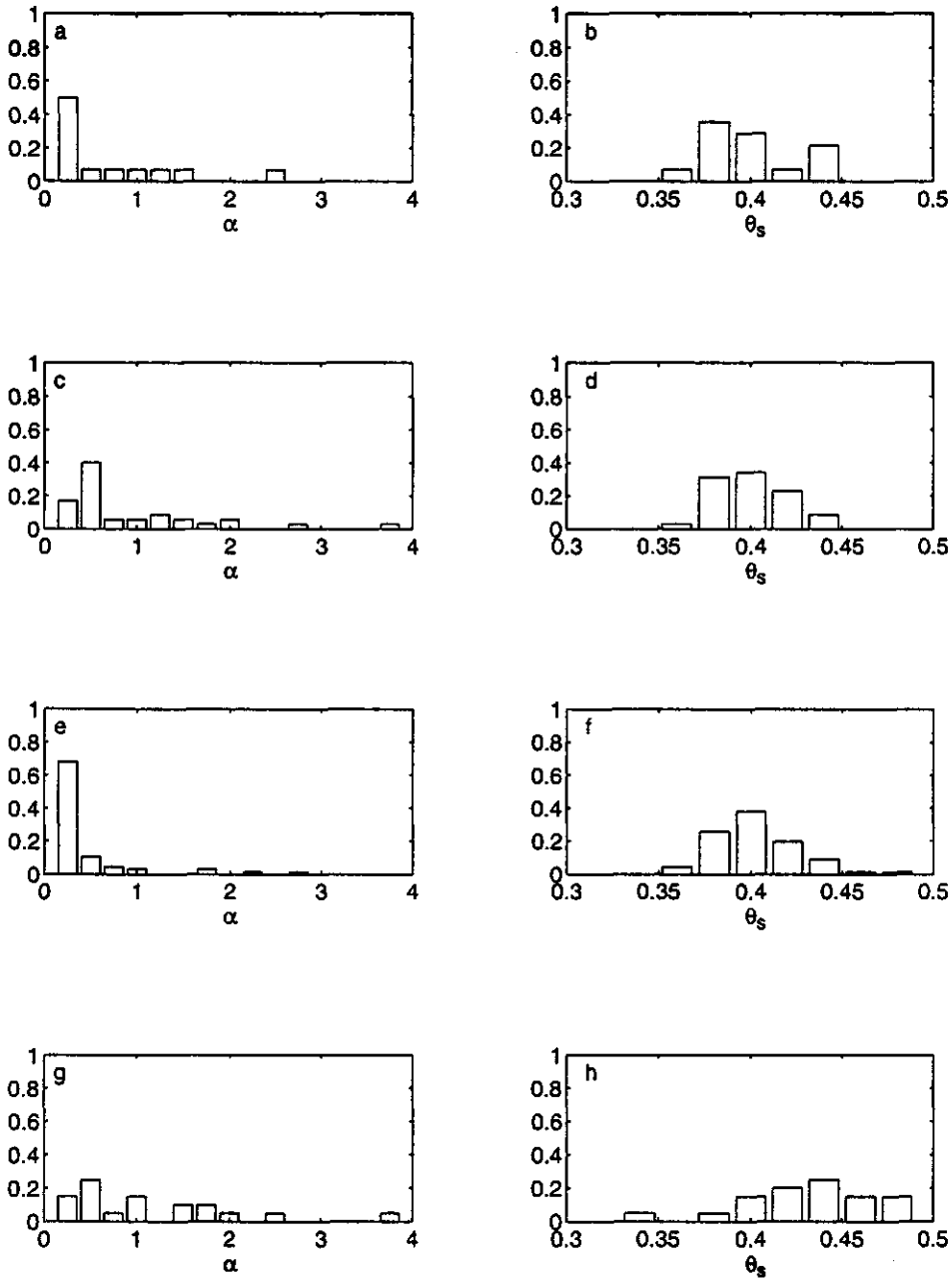

Figure 3.16: Frequency distributions of scaling factors α and saturated moisture contents θ_s of samples collected at BAR1 (a,b), BAR5 (c,d), Barrax (e,f) and Tomelloso (e,f).

Chapter 4

Conclusions

- **Root distribution and rooting depth**

  The studies of both the vine root system and the soil profiles at three Tomelloso sites show that the earlier assumption about shallow vine rooting depth was obviously incorrect. Root growth starts at about 30 cm depth in the sandy top soil, where the roots spread in all directions from a horizontal subsurface branch. The vine roots then penetrate vertically into the calcareous layer, concentrating in horizontal zones due to the structure of this layer. The calcareous layer continues over a certain depth which varies between locations and overlies a calcareous mudstone layer. If the mudstone layer starts at a shallow depth like at TOM4, the roots also penetrate into this layer along the loam filled fractures.

  The maximum rooting depth at the Tomelloso sites could not be determined. Taking into account the rooting depth observed at the gravel pit north of Tomelloso, it seems reasonable to assume that the vine roots reach depths of at least 3 meters.

- **Root water uptake**

  At all three sites root water uptake obviously takes place from the calcareous layer. Furthermore, it seems reasonable to assume that root water uptake also takes place from the mudstone layer. No quantitative information was obtained, however, on water availability and permeability for the calcareous and mudstone layers. Concerning the former, additional information may result from measurements by LTHE, Grenoble during the summer of 1994 which will be reported on elsewhere.

- **Soil hydraulic properties**

  The adjusted optimization procedure for the multistep outflow experiments yields a good agreement of optimized soil water retention curves with data measured in the field. The optimized saturated hydraulic conductivity, however, seems rather unrealistic and should be considered a fitting parameter more than a "true" field value.

Simultaneous scaling of $\ln h$ and $\ln k$ yields good results for soil water retention data for samples collected at Barrax. Scaling results for hydraulic conductivity curves are relatively poor, especially for all combined Barrax samples.

- **Modelling**

  For modelling purposes, an evaporation zone from 0-30 cm depth (sandy) and a transpiration zone (> 30 cm depth) can be distinguished. For this latter zone, however, the classical thinking of Darcy flow, characterizing a soil layer by its hydraulic functions $\theta(h)$ and $k(h)$, is very questionable. In the calcareous mudstone layer water flow seems possible only through the fractures between rock fragments, which should be accounted for in modelling.

  To include spatial variability of soil hydraulic properties in e.g. Monte Carlo simulations, the statistical distributions of $\ln \alpha$ and θ_s presented in 3.3 may be used.

Land use map of Tomelloso site, 1991

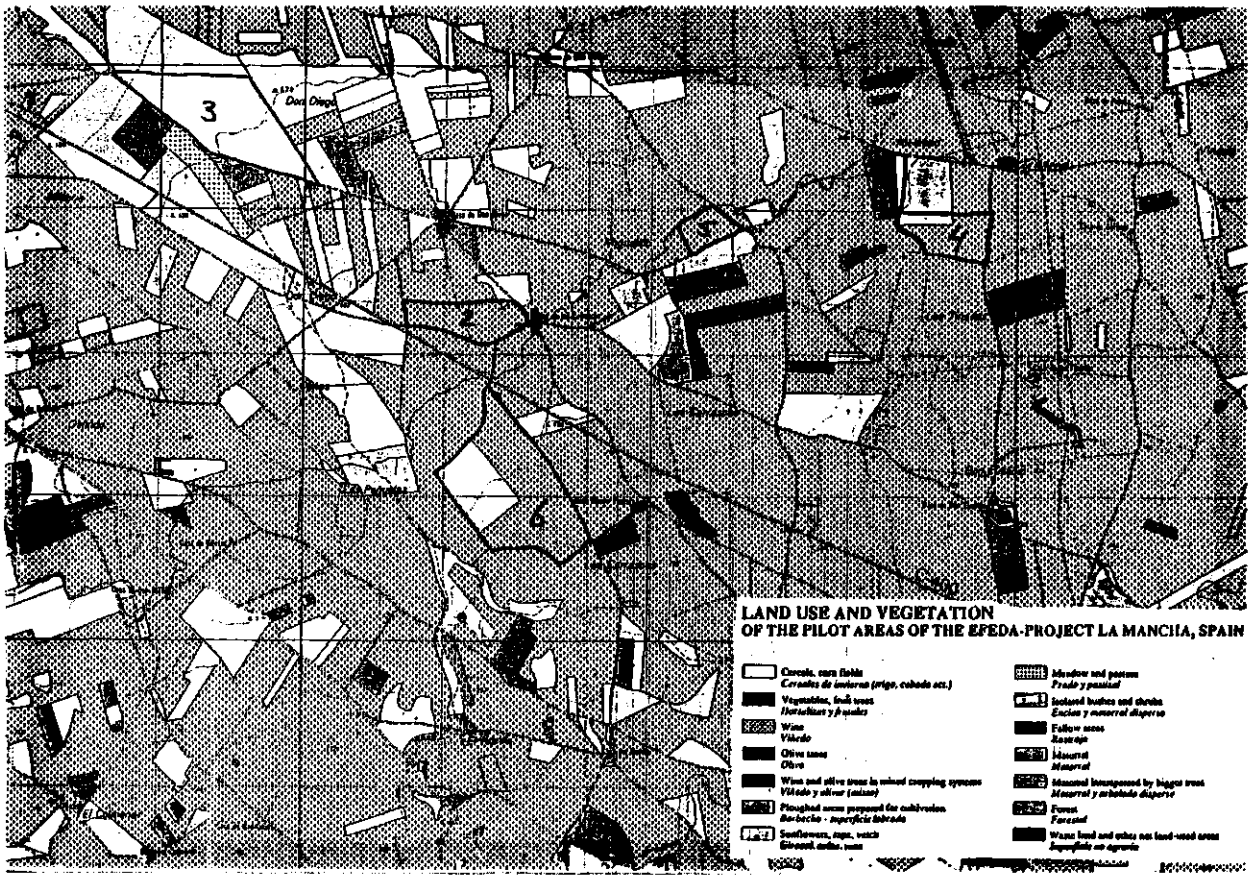

Part II

HAPEX-SAHEL

Chapter 6

INTRODUCTION

This second part of the HAPEX-Sahel basic report which describes the contributions of the Department of Water Resources, Wageningen Agricultural University, is related to the second objective being the characterization of soil hydraulic properties at selected locations within the West-Central Supersite. During the IOP numerous undisturbed soil samples of three different volumes were collected at different subsites and different depths as summarized in Report 37 [13] , appendix V. The hydraulic properties of these samples were determined according to the multistep outflow method [6, Van Dam *et al.*, 1994] which was described in Report 37 [13]. The analytical expressions introduced to describe the soil hydraulic properties are in this case the Mualem-Van Genuchten (MVG) expressions [8, Van Genuchten, 1980] which need at maximum 6 parameters to characterize the hydraulic properties (equation 48 and 49, Report 37 [13]). Important for a proper optimization procedure are a priori estimates of constraints and initial values of the parameters. In order to obtain correct estimates for all samples, several test runs were performed for 6 selected samples. The test runs covered different sets of constraints and initial values for the parameters. Apart from measured time-outflow data, additional information was included in the optimization process by introducing fixed retention data and separately measured conductivity data. The test runs resulted in a definition of the best performing set of constraints and initial values which was used for all collected samples.

Apart from the outflow experiments, soil texture analysis was performed for a number of samples. This was done because information about the grain size distribution may support the interpretation of the results of the multistep outflow optimizations. Grain size distributions are also used in pedo-transfer models which may be applied in future.

In addition to the sampling strategy applied in the field and the general setup of the multistep outflow method, which were already described in Report 37 [13], 2.5 and 3.5, chapter 7 of this report explains the specific settings during the optimization procedure of time-outflow data, the hydraulic conductivity measurements and the soil texture analysis. Chapter 8 gives the results of

the experiments and optimizations. First the outcome of the test runs will be discussed, followed by the optimization results for all collected samples. Finally grain size distributions of several samples will be shown.

For modelling purposes it is useful to transform the large data set of soil hydraulic properties for individual samples into a meaningful average while preserving the information on spatial variability of the original data set. This can be achieved through scaling, based upon the similar media theory [12, Miller and Miller, 1956]. Scaling results are presented in chapter 9.

Chapter 7

MATERIAL AND METHODS

7.1 Multistep outflow method

The multistep outflow measurements were performed in series of 20 (100 cc) or 10 (250 cc or 600 cc) samples. During a period of about 2 weeks, the pressure applied on top of the sample was increased stepwise until a pressure of 1000 cm water column was reached. During the experiment time and cumulative outflow were recorded.

After saturating the samples they were brought at equilibrium for $h_a = 15$ cm and the cumulative outflow between $h_a = 0$ cm and $h_a = 15$ cm pressure was collected. The actual experiment started at 15 cm pressure because the first step of the outflow experiment ($h_a = 0$ to 15 cm) often shows an irregular cumulative outflow which is probably caused by air entrapment and contribution of macro pores to the flow process [5, Van Dam *et al.*, 1990]. Then the pneumatic pressure was increased to respectively 30, 50, 100, 350 and finally to 1000 cm. At 1000 cm pressure, outflow was recorded until near-equilibrium was reached. After finishing the outflow experiment, the final moisture content was determined by weighing each sample before and after ovendrying at 106 °C during 24 hours.

For the simulation of time-outflow data and optimization of the MVG-parameters, the program "MULSTP" was used [5, Van Dam *et al.*, 1990]. In the optimization process 4 parameters were left variable: a_g, n, k_s and l. The saturated moisture content θ_s was determined from measured cumulative outflow between $h_a = 0$ cm and $h_a = 1000$ cm pressure and measured $\theta(h_a = 1000\,\text{cm})$ values. For a number of samples the moisture content was not measured after finishing the outflow experiment. In this case, an average $\theta(h_a = 1000$ cm) of 0.035 [$\text{cm}^3\,\text{cm}^{-3}$] was assumed. The average residual moisture content θ_r was set at 0.01 [$\text{cm}^3\,\text{cm}^{-3}$].

The range of possible values for the parameters n, k_s and l was limited in order to avoid problems during the optimization procedure. Values of n smaller

than 1 cause a physically unrealistic shape of the retention curve, whereas n-values larger than 5 may cause problems during the optimization procedure. Optimized values of k_s and l are highly correlated; not constraining their possible ranges may also cause unrealistic values for one or both parameters. Values of a_g should be larger than 0.

In order to obtain correct estimates of parameter constraints for all samples, several test runs were performed for each of 6 samples, collected at different subsites. The test runs differed in setting of parameter constraints and included data. Additional to measured time-outflow data, measured $\theta(h)$ points and separately measured $k(h)$ data were in some cases included. The results of the test runs were compared considering: 1. the agreement of measured and simulated time-outflow data and 2. the physical reality of the values of the optimized parameters k_s, a_g, l and n. The choice of the optimization setting influences both criteria.

7.2 Conductivity method

One of the optimized parameters for the multistep outflow experiments is the hydraulic conductivity at saturation k_s. To obtain direct information on hydraulic conductivity values, additional measurements of k were performed after finishing the outflow experiments. It was chosen to measure k at small negative pressures (-18 cm $< h <$ 0 cm) to eliminate the influence of macro pores.

A schematic diagram of the experimental setup is shown in Fig. 7.1. A soil sample is clamped between two porous plates by which water is supplied at identical small negative pressure heads. Under steady-state conditions, this pressure head exists over the entire soil column ($\partial h/\partial z = 0$), hence water flow is solely driven by gravity. The hydraulic gradient $\partial H/\partial z$ in this case equals 1 and according to Darcy's law the conductivity then equals the fluxdensity:

$$q = -k\frac{\partial H}{\partial z} \tag{7.1}$$

where q is fluxdensity [cm h^{-1}] and z is elevation head [cm].

Ideally, the applied hydraulic gradient would be fully available for the water flow through the soil column. In order to account for plate and tube resistances, however, the hydraulic heads at top and bottom of the soil column were measured by quickly responding micro tensiometers to ensure the existence of unit gradient.

After saturation of the soil column and de-aeration of all the tubing, the measurements started by recording time and cumulative outflow. The q_{in} was measured using a Mariotte buret to maintain a constant hydraulic head, the q_{out} was measured using a graduated cylinder. After reaching steady-state ($q_{in} = q_{out}$) the pressure head h was calculated from measured H and z.

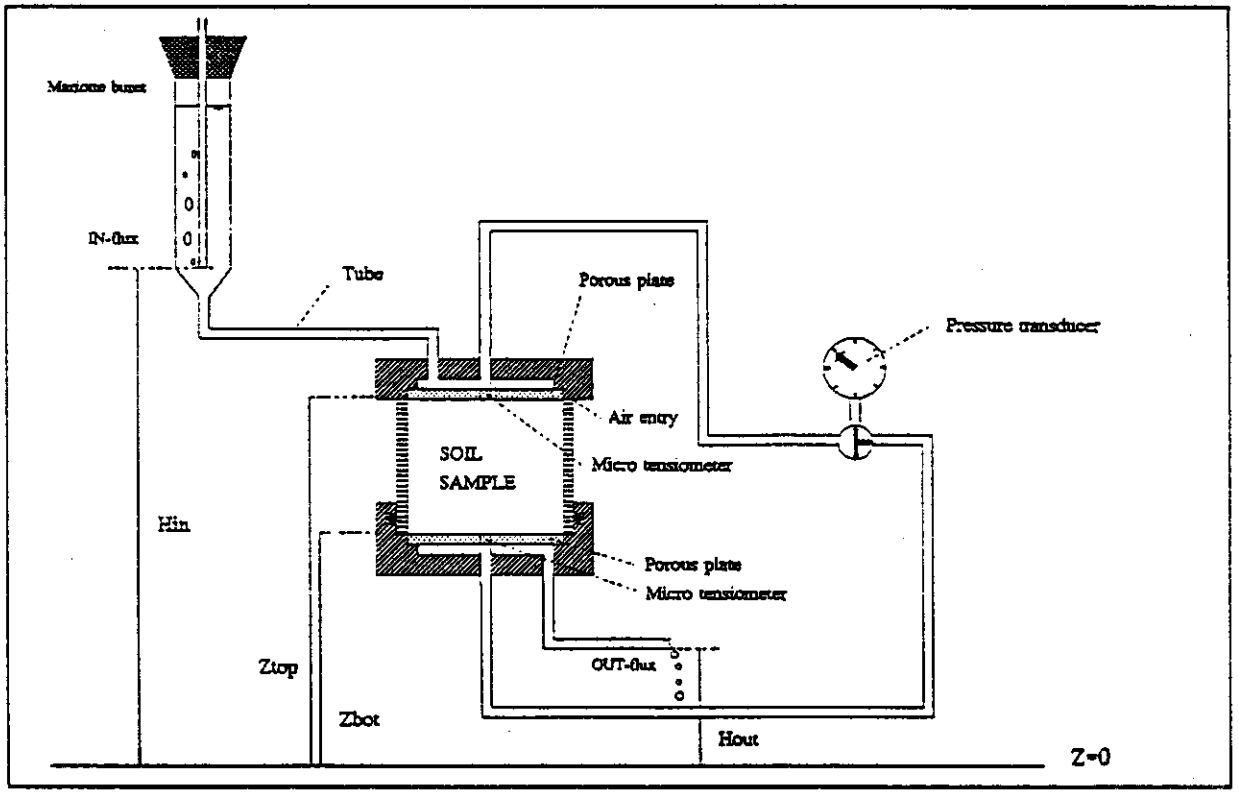

Figure 7.1: Experimental setup of hydraulic conductivity measurements

7.3 Grainsize distribution analysis

The grain size distribution of 29 undisturbed soil samples collected at different subsites was analyzed. From the degraded bush 12 samples were analyzed which characterize the typical transition from bare, eroded soil to vegetated, non-eroded soil. From the fallow bush 11 samples were analyzed which were collected in the vicinity of plots where soil moisture was monitored during the HAPEX-Sahel IOP. Additionally the samples selected for the multistep test runs were analyzed.

The texture analysis was performed according to [11, Klute, 1986]. After removing cementing compounds from a soil sample, the mass fractions of the grain sizes < 2, $2-16$, $16-50$, $50-106$, $106-125$, $125-212$, $212-425$, $425-2000$ and > 2000 μm were determined. A sample was divided into fractions $< 50\,\mu$m and $> 50\,\mu$m by wet-sieving. The fraction $> 50\,\mu$m was consequently sieved to obtain all separate mass fractions in this range. These separate mass fractions were determined using the known sedimentation speed of particles in water. The sedimentation speed of the particles is the resultant of two opposite forces: the gravitation and the friction due to movement in a liquid medium. Assuming the particles attain a terminal velocity almost instantly, the sedimentation speed can be determined according to Stokes' law:

$$\frac{s}{t} = \frac{2\left(\rho_s - \rho_l\right) g r^2}{9\eta} \tag{7.2}$$

with s is depth [cm] (water surface level $s = 0$), ρ_s and ρ_l are particle density (2.675 g cm^{-3}) and density of the medium (water: 1.000 g m^{-3}) respectively, g is gravity acceleration (9.81 m s^{-1}), r is mean particle radius [m], t is time [s] and η is the dynamic viscosity of the medium (1.005 x 10^{-3} Pa s at 20°C).

According to (7.2), particles $< 16\,\mu$m for which r equals 8.10^{-6} will be at 20.8 cm depth after 15 min and particles $< 2\,\mu$m will reach this depth after 16 h. Hence samples were collected at this depth and times using a pipette. After oven-drying the sample at 106°C for 24 hours, the mass fraction f_m was calculated according to:

$$f_m = \frac{1000d}{Vw} \tag{7.3}$$

with d is mass of the particle fraction [g], V is pipette volume [cm^3] and w is mass of oven-dry sample [g].

Chapter 8

RESULTS AND DISCUSSION

8.1 Conductivity measurements

The results of the conductivity measurements are shown in Table 8.1. The range of conductivity values near saturation appears to be quite small: at -5 cm pressure, k varies between 3 and 11 [cm h^{-1}]. Furthermore, the decrease in k over the measured pressure range is small which corresponds with results of the multistep outflow experiments, in which the average change of moisture content over the range 0 to -15 cm pressure was only 0.04 [cm^3 cm^{-3}].

Table 8.1: Measured conductivity values at small negative pressures

sample	h [cm]	k [cm h^{-1}]	sample	h [cm]	k [cm h^{-1}]
44	-5.1	10.6	76	-5.1	3.1
	-10.0	11.1		-14.5	0.7
77	-7.2	5.9	46	-10.7	7.6
	-12.7	5.3		-19.0	8.0
68	-1.0	6.0	7	-1.2	5.3
	-6.2	6.0		-8.5	5.6
	-14.0	5.5		-16.0	5.8
	-18.0	5.4			
64	-4.2	5.6	6	-4.2	5.6
	-10.3	5.4		-10.1	6.2
	-18.1	5.1		-17.5	5.5
70	-3.0	2.8	69	-4.3	5.6
	-9.1	3.2		-16.9	3.6
	-17.4	2.2			

Table 8.2: Settings for different optimization test runs

test	k_s [cm h^{-1}]	l [-]	fixed $\theta(h)$	k at -5 cm	k at -10 cm	k at -15 cm
1	$0-10$	-2 – 2.5	$h=15$			
2	$0-10$ >0	-2 – 2.5	$h=15$ $h=1000$			
3	>0	-2 – 2.5	$h=15$	$w=10$	$w=10$	$w=10$
4	>0	-2 – 2.5	$h=15$	$w=10$		
5	>0	-2 – 2.5	$h=15$			$w=10$
6	0-10	-2 – 2.5	$h=15$	$w=3$		
7	>0	-9.9 – 9.9	$h=15$	$w=10$	$w=10$	$w=10$
8	>0 >0	-2 – 2.5	$h=15$	$k=5.6$ $w=1$		

8.2 Multistep outflow experiments

8.2.1 Test runs

Eight test runs were performed in order to determine the optimal setting for the inverse modelling of the outflow experiments. The settings for the different test runs are given in Table 8.2.

in all cases $a_g > 0$, $1.1 \leq n \leq 5$, θ_r *and* θ_s *fixed*

The resulting simulated and measured time-outflow data for part of the test runs is shown in Figure 8.1. Resulting retention curves are shown in Figure 8.2 including the calculated moisture content at the end of each pressure step. In principle one may expect that the optimized retention curves will not yield moisture contents higher than those 'measured' points. Figure 8.3 shows measured and simulated conductivity data in the range near saturation.

Test 1, with no additional data included, yielded k_s-values equal to the upper constraint (10 cm h^{-1}) for 4 samples. A similar result was obtained running test 2. Measured outflow was simulated quite well for most samples in test 1 (Fig. 8.1). When a fixed retention point at $h = 1000$ cm was included (test 2) the root mean square error RMS of observed versus simulated time-outflow data increased.

Separately measured conductivity data were used in test 3 to 7. Including all measured k-values with a weighing factor $w = 10$ lead to satisfactory results when the range for l was practically non-restricted (test 7). Using a single k-value at $h = -5$ cm (test 4) or at $h = -15$ cm pressure (test 5) with $w = 10$ yielded quite a good representation of time-outflow data (Fig. 8.1) and measured conductivity values (Fig. 8.3) for most samples. However, when comparing RMS and k_s-values of test 4 and 5, test 4 yielded slightly better results. Reducing w to 3 for the k-value at $h = -5$ cm and limiting the k_s range from 0 to 10 cm h^{-1} (test 6) again lead to optimized k_s-values equal to the upper constraint.

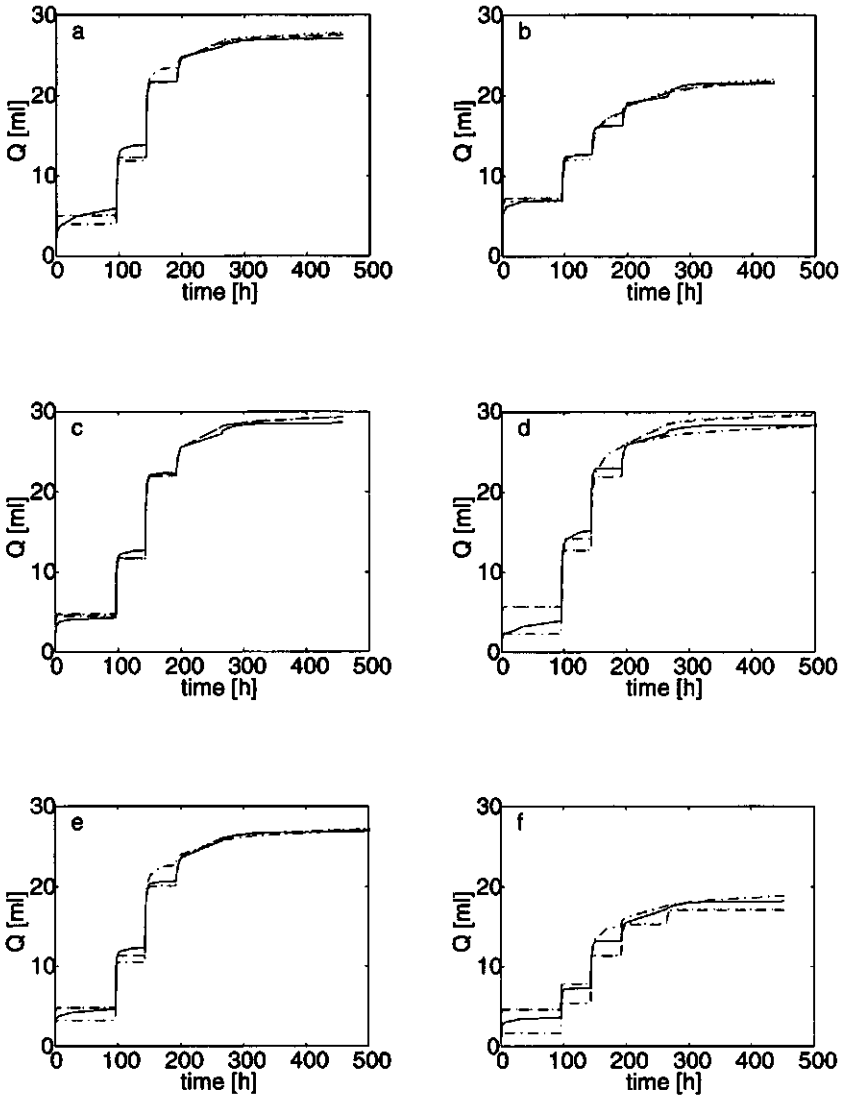

Figure 8.1: Measured (solid lines) and simulated time-outflow data for test 4 (dashed), test 7 (dash-dotted) and test 8 (dotted) of selected test samples (a) 44, (b) 76, (c) 69, (d) 46, (e) 68, (f) 7

Based upon the results of test 1 to 7 it seems most promising to include a single retention point at $h = -15$ cm and include an additional k-value near saturation without limiting k_s in the optimization procedure. However, measured conductivity data are not available for all collected samples. Since the range of measured k-values was quite small (Table 8.1) it was decided to use the average measured k-value at about -5 cm pressure with a weighing factor $w = 1$ and include this value in the optimization procedure of all samples. To avoid problems during the optimization process, l was restricted to the range $-2 \leq l \leq -2.5$. Results for the test samples using this setting are represented as test 8.

Compared to test 4, in which the actually measured k at $h = -5$ cm was used, test 8 yields satisfactory results except for sample 7. The problems in fitting time-outflow data for this sample, as is the case in all test runs, might be due to the relatively high outflow in the first pressure step ($h_a = 0$ to 15 cm) of the outflow experiment. Since only a few of the collected samples showed a similar outflow pattern no special attention was paid to this problem.

8.2.2 Final results

All samples measured by the multistep outflow method were optimized with the following constraints: $a_g > 0$, $1.1 \leq n \leq 5$, $\theta_r = 0.01$, and $-2 \leq l \leq 2.5$. The saturated moisture content θ_s was fixed at the value derived as given in 7.1. At $h = -5$ cm an additional k-value of 5.6 cm h^{-1} was included with $w = 1$. The resulting MVG-parameters for all measured 100 cm^3 soil samples are given in appendix **A**.

The final multistep outflow results were also compared with retention data measured directly in the field at a number of plots (see 3.2, part I). Figure 8.4 shows that the agreement between laboratory and field data is rather good with some deviation in the range $h > 200$, where field moisture contents are slightly higher than the optimized retention curves.

8.3 Texture analysis

8.3.1 Multistep test samples

The cumulative grain size distribution for the multistep test samples is shown in Figure 8.5. All test samples were collected at 0-5 cm depth.

The cumulative grain size distributions of sample 44 and 46 which were collected at the millet subsite and of sample 7, collected at the fallow bush subsite are quite similar. Sample 68 and 69 were both collected at a non-eroded location at the degraded bush subsite within a few meters distance and hence show similar cumulative grain size distributions. Sample 76 was collected at an eroded location at the degraded bush and apparently the mass fraction < 2 μm at this spot is relatively large compared to the other samples. This result

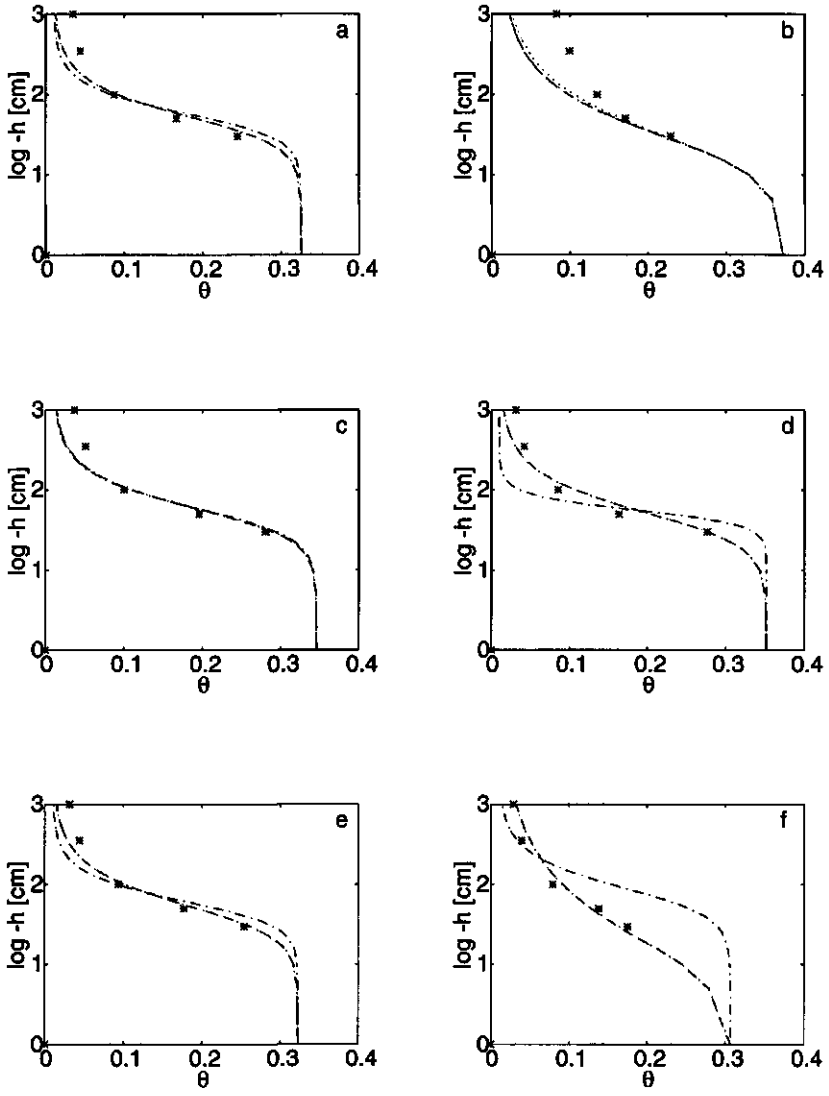

Figure 8.2: Simulated retention curves of test 4 (dashed), test 7 (dash-dotted), test 8 (dotted) and measured moisture content (∗) at end of pressure steps of selected test samples (a) 44, (b) 76, (c) 69, (d) 46, (e) 68 and (f) 7

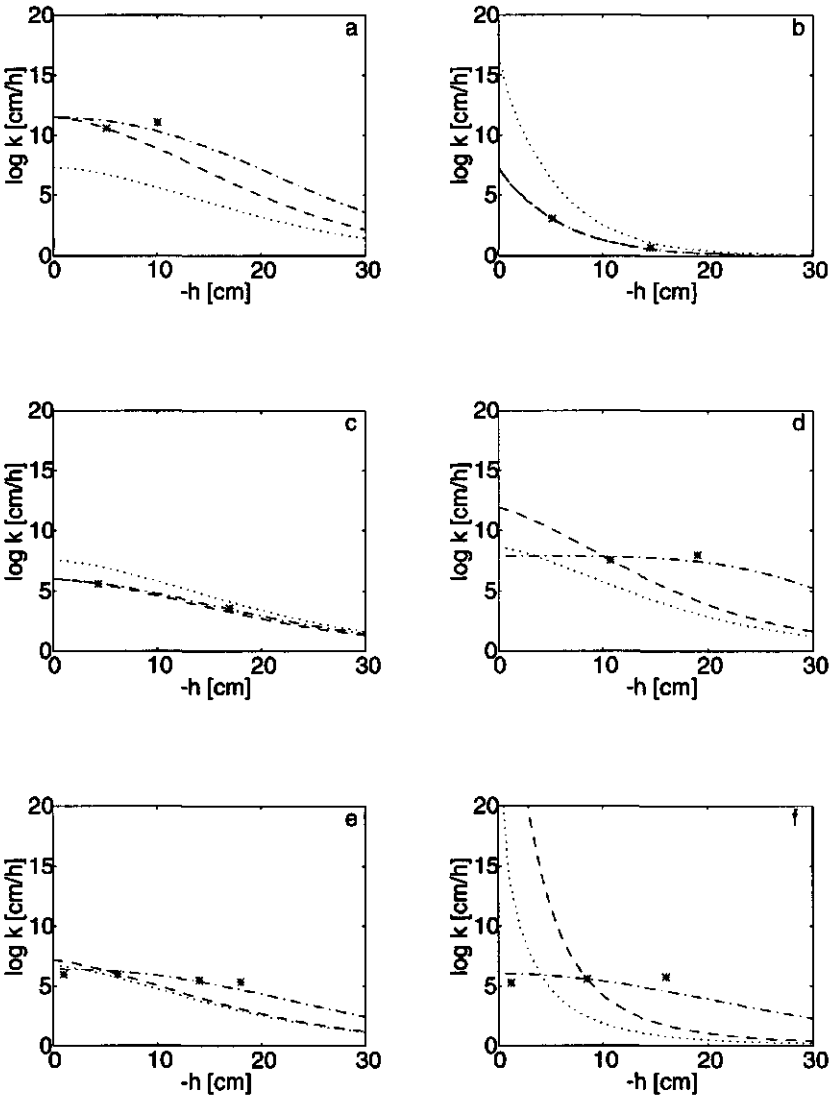

Figure 8.3: Simulated conductivity curves of test 4 (dashed), test 7 (dash-dotted) and test 8 (dotted) and measured data (*) near saturation for selected test samples (a) 44, (b) 76, (c) 69, (d) 46, (e) 68 and (f) 7

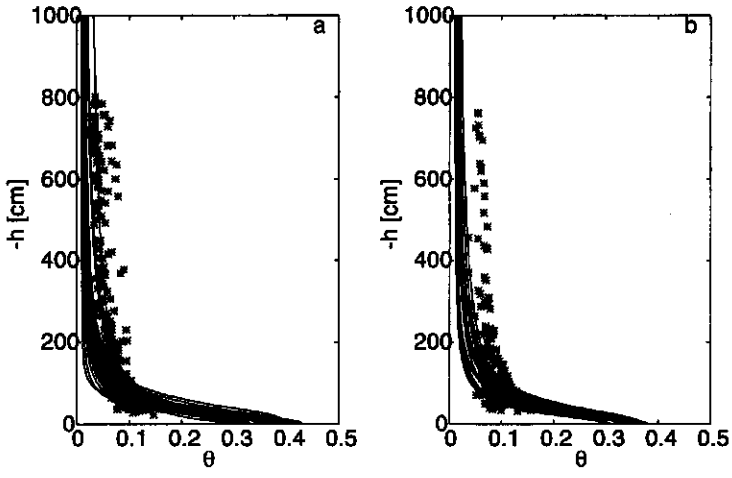

Figure 8.4: Simulated retention curves (solid lines) and field retention data (*) for (a) fallow bush subsite and (b) millet subsite

corresponds with the mechanisms of soil crusting at sandy sahelian soils as described by several authors (e.g. [3] Casenave and Valentin, 1992; [7], Van der Watt and Valentin, 1992). According to Van der Watt and Valentin [7, 1992] a dense surface seal composed of fine particles results from a sorting process due to raindrop impact followed by lateral particle transport caused by surface runoff. From field observations and grain size distribution results it seems obvious that this process indeed takes place at this specific subsite.

8.3.2 Fallow bush subsite

Five samples collected at the same location at different depths (near plot 30) were analyzed in order to obtain information about the variability of the grain size distribution with depth. Figure 8.6 shows that the contribution of the mass fraction < 2 μm slightly increases with depth.

In Appendix B the grain size distribution for a number of samples collected at the fallow bush is given. The average mass fraction < 2 μm is quite similar at 0-5 cm and 10-15 cm depth and slightly higher at 35-40 cm depth. At 0-5 cm depth there is relatively more difference between samples in the mass fraction < 2 μm, compared to the other depths.

8.3.3 Degraded bush subsite

As described in Report 37 [13], appendix V at the degraded bush subsite a transect was sampled at the characteristic transition from bare eroded soil to non-eroded soil. The grain size distributions of the samples collected at part

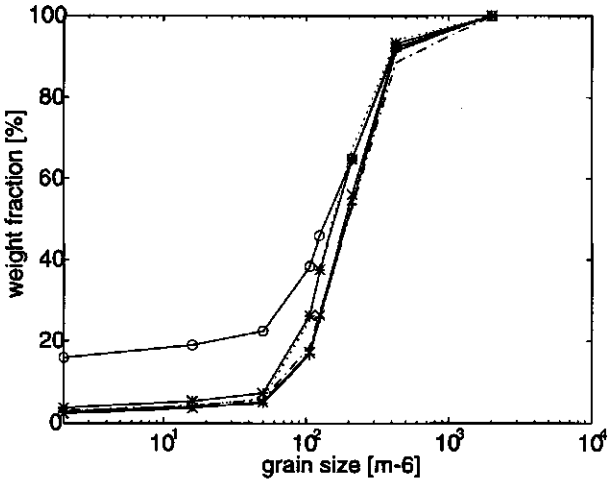

Figure 8.5: Cumulative grain size distribution of multistep test samples 44 (+), 76 (o), 69 (*), 46 (x), 68 (dotted) and 7 (dash-dotted)

1, 4, 6 and 10 of this transect were analyzed. Figure 8.7 shows results for the samples collected at 10-15cm depth, hence of the C-horizont in transect part 1 and 4 and of the non-eroded A-horizont in transect part 6 and 10. At the eroded location the mass fraction < 2 μm appears to be much higher than at the non-eroded location. Similar results were obtained at 15-25cm depth. All grain size distribution results are summarized in appendix 9.

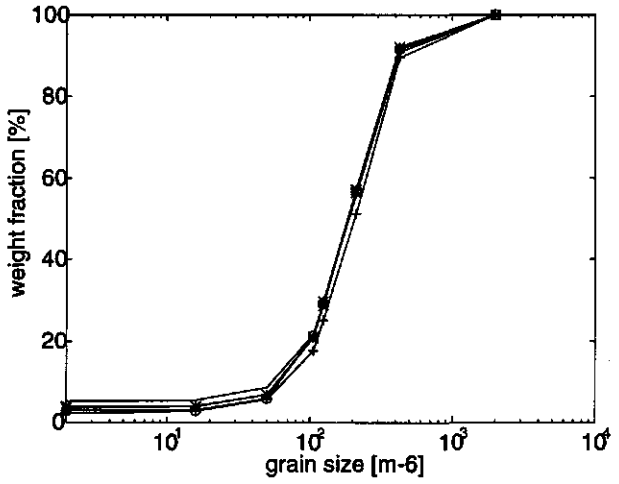

Figure 8.6: Cumulative grain size distribution of fallow bush samples collected at different depths near plot 30: 10-15 cm (+), 20-25 cm (o), 30-35 cm (*), 37-42 cm (x) and 45-50 cm depth (dotted)

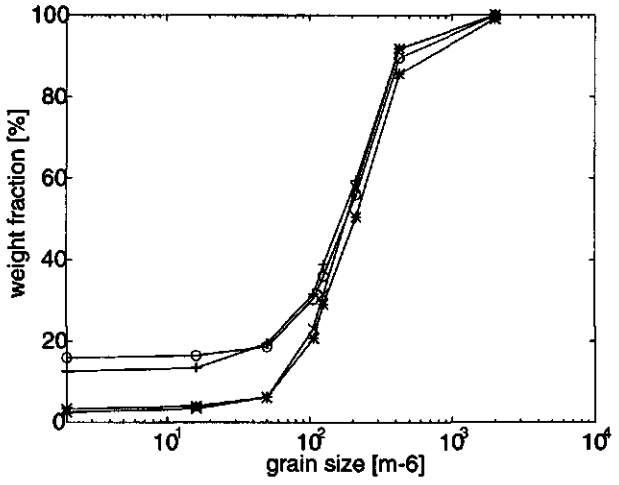

Figure 8.7: Cumulative grain size distribution of degraded bush samples collected at the transition from bare to non-eroded soil: transect part 1 (+), part 4 (o), part 6 (*) and part 10 (x)

Chapter 9

Scaling of soil hydraulic properties

The data set obtained from the multistep outflow experiments provides information on the spatial variability of the soil hydraulic properties in the HAPEX-Sahel area. For future modelling purposes it is useful to transform this large data set to a representative average while preserving the variability of individual sampling locations. This can be achieved through the application of geometric similar media theory [12, Miller and Miller, 1956].

For geometric similar media a scaling factor α_i can be defined as the ratio of the microscopic characteristic length λ_i of a soil at location i and the characteristic length of a reference soil λ^*:

$$\alpha_i = \lambda_i / \lambda^* \tag{9.1}$$

Scaling theory then results in a relation between the hydraulic properties of a sample collected at location i and a representative mean or reference curve. The relationships between the scaled mean soil matric head h^* and conductivity k^* and the hydraulic properties of sample i are given by:

$$h_i = h^* / \alpha_i \tag{9.2}$$

$$k_i = k^* \alpha_i^2 \tag{9.3}$$

Since in reality soils may not fully obey the concept of similar media, the scaling factors α_i in (9.2) and (9.3) can be different if retention and conductivity curves are scaled independently (e.g. [9], Hopmans, 1987). To obtain a single set of scaling factors both hydraulic functions were therefore scaled simultaneously using the algorithm described by [4, Clausnitzer *et al.*, 1992].

In addition to the results described in the previous sections, the hydraulic functions of 24 samples collected in 1991at a fallow site near Ouallam, approximately 100 km north of Niamey, were included in the scaling process. The sampling lay-out at the Ouallam site and the MVG-parameters for individual samples are given in appendix **C**. To study the variability between subsites, scaling was performed for each subsite individually and for all samples simultaneously. The scaled reference curves for individual subsites are presented in Fig. 9.1 and the statistical distribution of the scaling factors α_i is shown in Fig. 9.2. Obviously, the scaled retention curves for different subsites are almost identical. The scaled conductivity curves and the distribution of α_i differ slightly for different sites, especially for the Northern Satellite site. However, the number of samples N collected at the Northern Satellite site is only 9 whereas for the other sites $N \geq 24$ hence no strong conclusions should be drawn from these results.

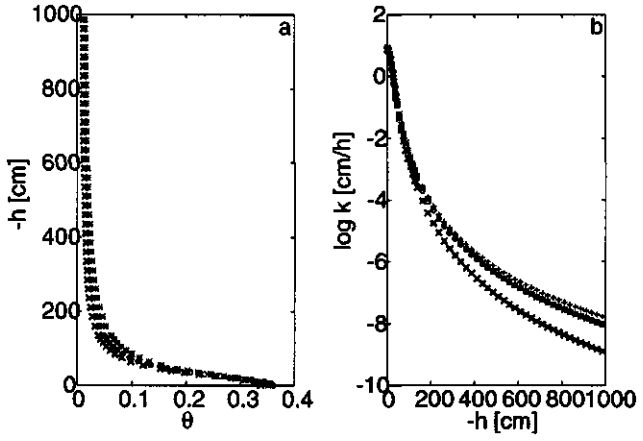

Figure 9.1: Scaled reference curves for subsite fallow bush (o), millet (+), degraded bush (*), Northern Satellite Site (dotted) and Ouallam site (x)

Since the results appeared quite similar for different subsites, it was decided to scale all samples simultaneously and derive a single set of scaling factors α_i and reference curves $\theta(h^*)$ and $k(h^*)$ (Table 9.1). An estimate for the success of the scaling procedure is given by the correlation between original and descaled h and k values as shown in Fig. 9.3. From Fig. 9.3 it is clear that scaling results are quite satisfactory for both soil water retention and hydraulic conductivity data.

The statistical distribution of the final set of scaling factors α_i and of the saturated moisture contents θ_s are given in Fig. 9.4. According to a Kolmogorov-Smirnoff test the distribution of $\ln \alpha$ and θ_s can be taken as normally distributed with mean μ and standard deviation σ (Table 9.1). A list of scaling factors for samples i is given in appendix **D**. For modelling of specific areas in the HAPEX-Sahel region one migth want to use separately derived reference curves, hence

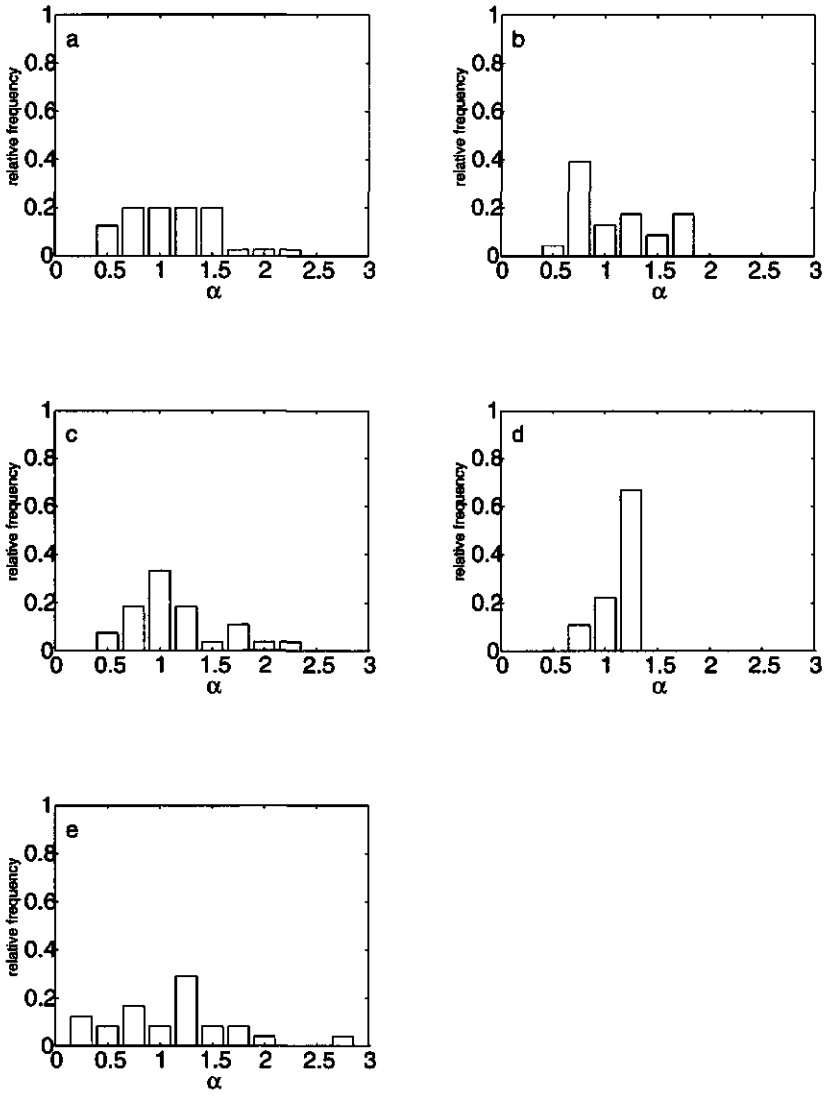

Figure 9.2: Frequency distribution of scaling factors α_i for subsite (a) fallow bush, (b) millet, (c) degraded bush, (d) Northern Satellite site and (e) Ouallam

results obtained by scaling data of individual subsites are also given in appendix 9.

Table 9.1: Parameters describing the final scaled reference curve and distribution of scaling factors and saturated moisture content

MVG-parameters						θ_s distribution		$\ln\alpha$ distribution	
a_g	n	θ_r	θ_s	k_s	l	μ	σ	μ	σ
0.0348	2.391	0.01	0.35	7.70	0.516	-0.35	0.03	-0.11	0.49

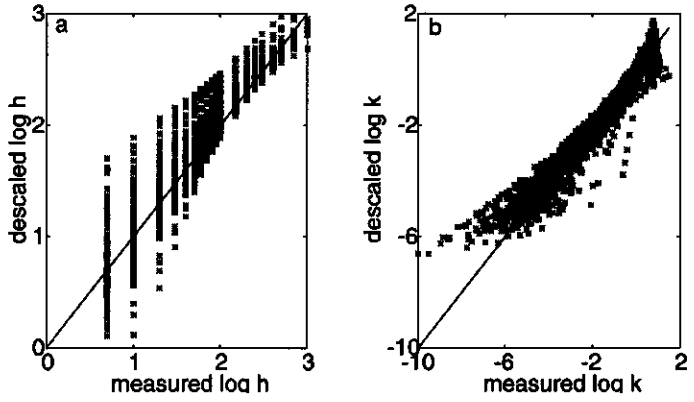

Figure 9.3: Correlation between original and descaled values of (a) pressure head and (b) hydraulic conductivity data

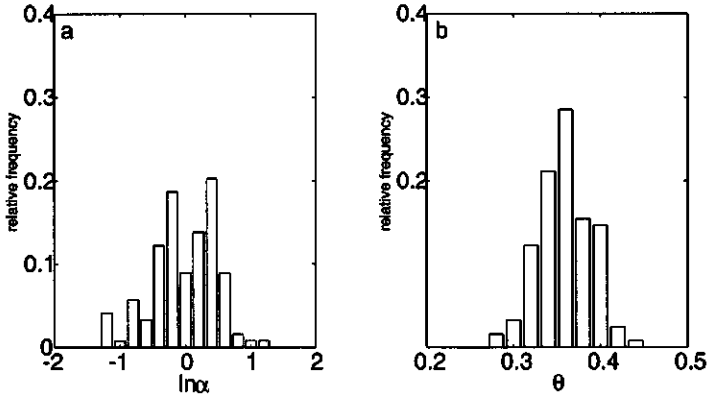

Figure 9.4: Frequency distribution of (a) scaling factors α_i and (b) saturated moisture content θ_s from simultaneous scaling of all samples

Bibliography

[1] W. Bohm. *Methods of Studying Root Systems*, volume 23 of *Ecological Series*. Springer-Verlag, Berlin, Germany, 1979.

[2] H.J. Bolle and B. Streckenbach (Eds.), editors. *The Echival Field Experiment in a Desertification Threatened Area (EFEDA)*., Germany, 1993. Free University of Berlin. Contract EPOC-CT 90-0030 Final Report.

[3] A. Casenave and C. Valentin. A runoff capability classification system based on surface features criteria in semi-arid areas of West Africa. *J. Hydrol.*, (130):231–249, 1992.

[4] V. Clausnitzer, J.W. Hopmans, and D.R. Nielsen. Simultaneous scaling of soil water retention and hydraulic conductivity curves. *Water Resources Res.*, (28):19–31, 1992.

[5] J.C. Van Dam, J.N.M. Stricker, and P. Droogers. From one-step to multistep. determinaion of soil hydraulic functions by outflow experiments. Technical Report 7, Dept. of Water Resources, Wageningen Agricultural University, 1990.

[6] J.C. Van Dam, J.N.M. Stricker, and P. Droogers. Inverse method to determine soil hydraulic functions from multistep outflow experiments. *Soil Sci. Soc. Am. J.*, (58):647–652, 1994.

[7] H.V.H. Van der Watt and C. Valentin. Soil crusting: The African view. In M.E. Sumner and B.A. Stewart, editors, *Soil Crusting: Chemical and Physical Processes*, pages 301–337, Boca raton, USA, 1992. Lewis Publishers.

[8] M. Th. Van Genuchten. A closed-form equation for predicting the hydraulic conductivity of unsaturated soils. *Soil Sci. Soc. Am. j.*, (44):892–898, 1980.

[9] J.W. Hopmans. A comparison of various methods to scale soil hydraulic properties. *J. Hydrol.*, (93):241–256, 1987.

[10] ISRIC. *TSBG: A Handbook of Methods*. ISRIC, Wageningen, The Netherlands, 1992.

[11] A. Klute. *Physical and Mineralogical Methods.* Madison, Wisconsin, USA, 2nd edition, 1986.

[12] E.E. Miller and R.D. Miller. Physical theory for capillary flow phenomena. *J. Appl. Phys.*, 27(4):324–332, 1956.

[13] P.Droogers, G.D. Van de Abeele, J. Cobbaert, C.P. Kim, R. R/O"sslerova, M.Soet, and J.N.M. Stricker. Basic data sets description and preliminary results of EFEDA-Spain. Technical report 37, Dept. of Water Resources, Wageningen Agricultural University, 1993.

Appendix A

Final MVG-parameter set for West Central Supersite

sample	site	plot	depth	α_g	n	θ_r	θ_s	k_s	l	RMS
1	1	-1	0	0.0205	2.383	0.01	0.28	6.09	1.49	1.122
2	1	-1	0	0.0270	2.364	0.01	0.35	7.90	1.14	1.097
3	1	-1	0	0.0355	1.979	0.01	0.37	8.33	1.28	1.371
4	1	-1	0	0.0323	1.980	0.01	0.31	8.39	0.85	1.327
5	1	-1	0	0.0348	1.975	0.01	0.35	8.43	0.37	1.588
6	1	-1	0	0.0348	1.932	0.01	0.30	9.10	0.16	1.289
7	1	-1	0	0.0939	1.571	0.01	0.31	25.42	-1.21	1.117
8	1	21	10	0.0307	2.270	0.01	0.36	6.90	0.69	0.942
9	1	22	10	0.0228	2.604	0.01	0.37	6.57	1.57	0.948
10	1	23	10	0.0301	2.653	0.01	0.37	6.34	0.93	1.049
11	1	24	10	0.0253	2.918	0.01	0.39	6.48	1.61	0.891
12	1	25	10	0.0225	4.559	0.01	0.31	5.98	1.33	0.831
13	1	26	10	0.0212	2.740	0.01	0.40	7.25	2.29	0.927
14	1	27	10	0.0456	2.390	0.01	0.39	8.09	0.19	1.121
15	1	28	10	0.0363	2.456	0.01	0.42	6.62	0.17	1.094
16	1	29	10	0.0373	2.373	0.01	0.38	6.42	0.20	1.700
17	1	30	10	0.0283	2.610	0.01	0.39	6.58	1.13	1.014
18	1	101	10	0.0347	2.150	0.01	0.29	7.68	0.97	0.813
19	1	102	10	0.0345	2.444	0.01	0.33	6.79	0.31	0.737
20	1	103	10	0.0378	2.133	0.01	0.32	8.07	0.24	1.134
21	1	104	10	0.0381	2.195	0.01	0.33	7.66	0.31	1.403
22	1	105	10	0.0333	2.342	0.01	0.33	7.18	0.42	1.258
23	1	106	10	0.0322	2.508	0.01	0.35	6.18	0.36	1.228
24	1	107	10	0.0297	2.412	0.01	0.36	6.71	0.51	1.617
25	1	108	10	0.0318	2.318	0.01	0.37	7.16	0.43	1.487
26	1	109	10	0.0344	2.588	0.01	0.37	6.87	0.39	0.771
27	1	110	10	0.0492	1.992	0.01	0.31	10.11	0.56	0.979
28	1	30	20	0.0278	2.416	0.01	0.36	6.72	0.88	0.760
29	1	30	30	0.0428	2.489	0.01	0.36	7.08	-0.00	0.843
30	1	21	35	0.0375	2.378	0.01	0.41	6.97	0.31	1.622
31	1	22	35	0.0369	2.622	0.01	0.40	6.74	0.19	1.320
32	1	23	35	0.0398	2.562	0.01	0.39	7.04	0.19	1.310
33	1	24	35	0.0433	3.056	0.01	0.43	6.53	-0.14	0.792
34	1	25	35	0.0441	2.586	0.01	0.39	7.71	-0.05	0.866
35	1	26	35	0.0424	2.127	0.01	0.39	8.84	0.13	1.393
36	1	27	35	0.0444	2.714	0.01	0.39	6.51	0.01	0.717
37	1	28	35	0.0452	2.513	0.01	0.39	7.17	0.36	1.302
38	1	29	35	0.0369	2.614	0.01	0.41	5.89	0.12	1.903
39	1	30	37	0.0410	2.542	0.01	0.36	6.25	0.10	1.040
40	1	30	45	0.0386	2.484	0.01	0.38	6.86	0.28	1.607
41	2	-1	0	0.0290	2.474	0.01	0.36	6.94	0.68	1.317
42	2	-1	0	0.0253	2.415	0.01	0.30	6.98	1.23	0.677
43	2	-1	0	0.0254	2.305	0.01	0.37	7.24	1.78	1.481
44	2	-1	0	0.0237	2.508	0.01	0.33	7.34	1.38	0.951
45	2	-1	0	0.0266	2.252	0.01	0.32	8.44	1.01	1.309

sample	site	plot	depth	α_g	n	θ_r	θ_s	k_s	l	RMS
46	2	-1	0	0.0257	2.276	0.01	0.35	8.69	1.15	1.809
47	2	1	10	0.0230	3.107	0.01	0.35	6.27	1.01	0.835
48	2	2	10	0.0268	2.384	0.01	0.34	6.81	1.07	1.516
49	2	3	10	0.0311	2.592	0.01	0.33	6.63	0.67	1.075
50	2	4	10	0.0298	2.278	0.01	0.32	7.22	0.80	1.179
51	2	5	10	0.0449	1.973	0.01	0.38	8.73	-0.87	1.989
52	2	6	10	0.0280	2.696	0.01	0.34	6.55	0.78	0.571
53	2	9	10	0.0349	2.208	0.01	0.34	8.09	0.54	1.018
54	2	1	25	0.0349	2.108	0.01	0.33	7.61	0.94	0.965
55	2	1	35	0.0425	1.845	0.01	0.31	9.83	-0.48	1.651
56	2	2	35	0.0479	2.346	0.01	0.35	7.97	-0.04	0.670
57	2	3	35	0.0406	2.688	0.01	0.34	6.68	1.32	0.836
58	2	4	35	0.0434	2.217	0.01	0.34	7.93	-0.12	1.127
59	2	5	35	0.0480	2.485	0.01	0.34	7.27	0.06	0.647
60	2	6	35	0.0461	2.367	0.01	0.30	7.40	-0.10	0.606
61	2	7	35	0.0456	2.474	0.01	0.38	7.11	-0.47	1.115
62	2	8	35	0.0509	2.403	0.01	0.37	7.66	-0.52	0.880
63	2	9	35	0.0405	2.643	0.01	0.37	6.82	-0.22	1.107
64	3	-1	0	0.0179	2.835	0.01	0.28	4.42	1.32	0.628
65	3	-1	0	0.0196	2.839	0.01	0.34	5.37	1.35	0.546
66	3	-1	0	0.0180	2.550	0.01	0.32	5.87	2.14	0.626
67	3	-1	0	0.0250	2.347	0.01	0.37	6.20	1.22	0.921
68	3	-1	0	0.0239	2.324	0.01	0.32	6.69	1.39	0.580
69	3	-1	0	0.0220	2.436	0.01	0.35	7.47	1.69	0.748
70	3	-1	0	0.0308	2.190	0.01	0.35	8.05	0.54	0.482
71	3	-1	0	0.0450	2.003	0.01	0.35	10.48	2.84	0.718
72	3	-1	0	0.0544	1.883	0.01	0.36	11.19	-0.53	0.461
73	3	-1	0	0.0441	2.001	0.01	0.39	11.29	1.46	0.964
74	3	-1	0	0.0522	1.835	0.01	0.34	11.49	-0.69	0.756
75	3	-1	0	0.0451	1.876	0.01	0.35	11.74	1.21	0.706
76	3	-1	0	0.0543	1.775	0.01	0.37	16.43	2.20	0.810
77	3	-1	0	0.0655	1.610	0.01	0.36	22.62	0.92	0.565
78	3	109	6	0.0259	2.440	0.01	0.32	6.45	1.21	0.530
79	3	106	7	0.0350	2.466	0.01	0.35	6.51	0.47	0.674
80	3	110	7	0.0374	2.065	0.01	0.39	8.48	-0.12	1.293
81	3	107	8	0.0271	2.594	0.01	0.37	7.01	0.44	0.563
82	3	101	10	0.0277	2.211	0.01	0.33	7.38	1.68	0.630
83	3	102	10	0.0397	2.400	0.01	0.36	7.38	-0.16	0.912
84	3	103	10	0.0406	2.568	0.01	0.37	6.87	-0.05	0.798
85	3	104	10	0.0465	2.344	0.01	0.35	7.87	-0.05	0.586
86	3	106	20	0.0368	2.111	0.01	0.37	8.35	-0.27	1.210
87	3	107	21	0.0318	2.578	0.01	0.36	6.93	0.49	0.575
88	3	108	21	0.0215	2.591	0.01	0.35	6.19	1.58	0.792
89	3	109	21	0.0221	2.637	0.01	0.32	5.96	1.30	0.449
90	3	110	21	0.0301	2.255	0.01	0.39	7.27	0.43	1.107
91	4	-1	0	0.0334	2.534	0.01	0.39	6.07	-0.62	0.962
92	4	-1	0	0.0224	3.755	0.01	0.35	6.34	0.65	0.880
93	4	-1	0	0.0271	2.713	0.01	0.36	7.03	0.47	0.835
94	4	-1	0	0.0214	5.000	0.01	0.33	7.11	1.27	0.976
95	4	2	30	0.0340	2.533	0.01	0.39	6.69	-0.60	1.090
96	4	4	30	0.0507	2.250	0.01	0.33	7.42	-0.97	0.643
97	4	5	30	0.0554	2.057	0.01	0.31	9.22	-0.82	0.648
98	4	7	30	0.0370	2.505	0.01	0.31	8.87	-0.76	0.769
99	4	9	30	0.0323	2.183	0.01	0.27	6.98	0.19	0.568

subsite fallow bush = 1, millet = 2, degraded bush = 3, Northern Satellite site = 4, Ouallam = 5

plot number: 1-64 neutron probe access tube, >100 transect part, -1 disc permeameter location

Appendix B

Grain size distribution analysis

				weight fraction [%]								
sample	plot	site	depth [cm]	<2	2-16	16-50	50-106	106-125	125-212	212-425	425-2000	>2000
82	101	3	10	12.52	0.90	5.98	12.24	7.13	20.74	32.39	8.11	0.00
B16	101	3	15	15.41	1.19	2.55	14.28	6.91	21.51	30.28	7.66	0.20
85	104	3	10	15.92	0.49	2.19	11.70	5.64	19.98	33.54	10.44	0.10
B6	104	3	10	13.77	1.14	2.26	11.72	6.18	20.20	34.11	10.62	0.00
79	106	3	7	3.31	0.72	2.20	14.46	8.34	21.54	35.00	13.58	0.58
86	106	3	20	5.02	0.95	3.56	17.07	8.06	24.11	32.52	8.66	0.05
B4	106	3	20	6.94	1.26	3.17	16.63	7.98	24.33	31.03	8.62	0.05
80	110	3	7	2.54	0.83	2.82	16.95	8.37	26.41	33.91	8.17	0.00
90	110	3	21	4.77	1.50	4.42	18.98	8.47	25.16	29.36	7.34	0.00
B23	110	3	22	5.57	1.22	3.86	16.42	7.19	24.05	33.03	8.66	0.00
74	-1	3	0	6.49	1.59	3.38	15.10	9.15	22.40	29.09	12.37	0.43
67	-1	3	0	2.45	0.64	2.91	17.99	9.02	27.18	31.39	8.41	0.00
8	21	1	10	1.78	0.04	2.90	13.01	10.31	28.74	35.12	8.11	0.00
30	21	1	35	5.18	0.01	3.52	14.63	10.42	26.20	31.96	8.09	0.00
11	24	1	10	2.44	0.01	3.15	12.90	9.00	26.75	35.45	10.30	0.00
33	24	1	35	6.74	0.06	2.35	12.99	8.51	26.63	33.75	8.96	0.00
15	28	1	10	2.84	0.00	2.97	14.33	8.34	25.66	35.52	10.33	0.00
37	28	1	35	5.86	0.01	2.36	11.28	7.83	23.51	36.87	12.28	0.00
17	30	1	10	2.31	0.53	2.88	11.93	7.48	26.03	38.33	10.50	0.00
28	30	1	20	2.93	0.01	2.97	15.44	7.84	27.50	34.83	8.48	0.00
29	30	1	30	3.52	0.46	2.84	14.09	8.64	27.66	34.84	7.95	0.00
39	30	1	37	3.95	0.01	3.00	14.09	7.64	27.81	35.73	7.77	0.00
40	30	1	45	5.24	0.26	3.14	13.05	7.81	26.25	35.04	9.21	0.00
44	-1	2	0	2.76	1.23	0.99	11.79	9.01	27.96	37.73	8.53	0.00
76	-1	3	0	15.89	3.14	3.51	15.86	7.60	19.03	27.21	7.68	0.08
69	-1	3	0	3.65	1.75	1.94	19.01	11.26	27.22	28.47	6.63	0.08
46	-1	2	0	2.32	1.36	1.56	12.03	9.22	29.63	36.33	7.56	0.00
68	-1	3	0	2.62	1.60	1.81	19.03	12.94	29.30	28.77	5.94	0.00
7	-1	1	0	3.05	1.24	1.58	12.72	8.67	25.59	35.82	11.34	0.00
42	-1	2	0	2.70	0.04	3.64	11.44	7.74	24.72	36.49	13.18	0.05
3	-1	1	0	2.58	1.13	3.16	13.31	10.15	24.46	31.69	13.51	0.00
4	-1	1	0	1.32	0.65	2.63	13.43	9.40	24.98	34.48	13.12	0.00
50	4	2	10	1.01	0.59	1.78	13.85	10.43	32.44	33.90	6.00	0.00

subsite fallow bush = 1, millet = 2, degraded bush = 3, Northern Satellite site = 4, Ouallam = 5

plot number: 1-64 neutron probe access tube, >100 transect part, -1 disc permeameter location

sample numbers starting with B, volume 600 cm3, all others 100 cm3

Appendix C

Sampling location and hydraulic properties at Ouallam site

sample	site	plot	depth	α_g	n	θ_r	θ_s	k_s	l	RMS
100	5	1	10	0.0359	2.309	0.01	0.33	7.07	1.18	0.666
101	5	2	10	0.0346	2.813	0.01	0.34	6.06	-1.26	1.496
102	5	3	10	0.0457	2.117	0.01	0.33	8.54	0.21	0.738
103	5	4	10	0.0311	2.327	0.01	0.34	6.77	1.79	0.842
104	5	5	10	0.0270	3.299	0.01	0.34	5.73	1.03	0.600
105	5	6	10	0.0306	2.912	0.01	0.34	5.90	-0.44	1.130
106	5	7	10	0.0343	3.385	0.01	0.34	5.71	-2.00	1.363
107	5	8	10	0.0942	1.606	0.01	0.34	34.11	1.01	0.282
108	5	9	10	0.0372	2.253	0.01	0.35	7.31	0.87	0.951
109	5	10	10	0.0306	2.884	0.01	0.35	5.95	0.56	1.079
110	5	11	10	0.0347	2.251	0.01	0.33	7.15	1.00	0.944
111	5	12	10	0.0305	2.680	0.01	0.34	6.15	0.77	1.107
112	5	13	10	0.0295	2.517	0.01	0.34	6.27	0.54	1.110
113	5	14	10	0.0273	3.598	0.01	0.33	5.66	1.36	0.984
114	5	15	10	0.0334	2.907	0.01	0.36	5.97	-0.78	1.484
115	5	16	10	0.0337	2.632	0.01	0.36	6.26	0.09	0.818
116	5	17	10	0.0431	2.587	0.01	0.33	6.58	-1.60	1.490
117	5	18	10	0.0288	2.868	0.01	0.33	5.90	-0.13	1.236
118	5	19	10	0.0282	3.059	0.01	0.36	5.81	0.83	1.082
119	5	20	10	0.0285	2.778	0.01	0.31	5.98	0.57	1.252
120	5	21	10	0.0342	2.049	0.01	0.32	8.15	2.50	0.895
121	5	22	10	0.0367	2.499	0.01	0.34	6.62	0.41	0.939
122	5	23	10	0.0302	2.243	0.01	0.34	6.97	2.45	0.973
123	5	24	10	0.0371	1.959	0.01	0.32	9.10	2.50	0.858

Appendix D

Scaling factors and reference curves

MVG-parameters of reference curves obtained by scaling all sites simultaneously and scaling of individual subsites

site	a_g	n	θ_r	θ_s	k_s	l	sample
all	0.0348	2.391	0.01	0.35	7.70	0.52	1-123
1	0.0356	2.381	0.01	0.36	7.57	0.49	1-40
2	0.0349	2.363	0.01	0.34	7.49	0.43	41-63
3	0.0326	2.250	0.01	0.35	8.54	0.89	64-90
4	0.0350	2.502	0.01	0.34	7.09	-0.27	91-99
5	0.0333	2.603	0.01	0.34	7.47	0.60	100-123

Scaling factors α_i obtained by scaling all sites simultaneously

sample	α	sample	α	sample	α	sample	α
1	0.567	33	2.312	65	0.841	97	0.999
2	0.736	34	1.69	66	0.557	98	1.451
3	0.393	35	0.794	67	0.645	99	0.716
4	0.407	36	1.818	68	0.596	100	0.806
5	0.445	37	1.457	69	0.63	101	1.878
6	0.429	38	1.39	70	0.68	102	0.805
7	0.379	39	1.427	71	0.286	103	0.641
8	0.731	40	1.265	72	0.598	104	1.343
9	0.755	41	0.94	73	0.492	105	1.678
10	1.092	42	0.724	74	0.475	106	2.73
11	0.958	43	0.564	75	0.369	107	0.283
12	1.438	44	0.759	76	0.247	108	0.806
13	0.706	45	0.637	77	0.268	109	1.405
14	1.326	46	0.633	78	0.753	110	0.745
15	1.184	47	1.156	79	1.11	111	1.144
16	1.074	48	0.743	80	0.637	112	1.011
17	0.992	49	1.111	81	1.058	113	1.225
18	0.632	50	0.717	82	0.528	114	1.816
19	1.098	51	0.656	83	1.248	115	1.365
20	0.733	52	1.108	84	1.515	116	1.982
21	0.832	53	0.752	85	1.311	117	1.454
22	0.916	54	0.595	86	0.753	118	1.253
23	1.104	55	0.435	87	1.159	119	1.258
24	0.906	56	1.344	88	0.729	120	0.337
25	0.857	57	1.132	89	0.792	121	1.202
26	1.276	58	0.997	90	0.738	122	0.456
27	0.644	59	1.572	91	1.338	123	0.286
28	0.819	60	1.345	92	1.527		
29	1.442	61	1.614	93	1.165		
30	1.077	62	1.646	94	1.621		
31	1.411	63	1.685	95	1.366		
32	1.422	64	0.752	96	1.343		